

An Active-Sterile Neutrino Transformation Solution for r -Process Nucleosynthesis

G. C. McLaughlin*, J.M. Fetter†, A.B. Balantekin‡, and G.M. Fuller§
*Institute for Nuclear Theory, University of Washington, Box 351550
Seattle, WA 98195-1550 USA*

Abstract

We discuss how matter-enhanced active-sterile neutrino transformation in the $\nu_e \rightleftharpoons \nu_s$ and $\bar{\nu}_e \rightleftharpoons \bar{\nu}_s$ channels could enable the production of the rapid neutron capture (r -process) nuclei in neutrino-heated supernova ejecta. In this scheme the lightest sterile neutrino would be heavier than the ν_e and split from it by a vacuum mass-squared difference of $3 \text{ eV}^2 \lesssim \delta m_{es}^2 \lesssim 70 \text{ eV}^2$ with vacuum mixing angle $\sin^2 2\theta_{es} > 10^{-4}$.

14.60.Pq, 14.60.St, 26.30.+k, 97.60.Bw

Typeset using REVTeX

*Current Address: TRIUMF, 4004 Wesbrook Mall, Vancouver, B.C., Canada, V6T2A3. Electronic address: gail@alph01.triumf.ca

†Current Address: Department of Physics, University of Wisconsin, Madison, Wisconsin 53706. Electronic address: fetter@nucth.physics.wisc.edu

‡Permanent Address: Department of Physics, University of Wisconsin, Madison, Wisconsin 53706. Electronic address: baha@nucth.physics.wisc.edu

§Permanent address: Department of Physics, University of California, San Diego La Jolla, CA 92093-0319. Electronic address: gfuller@ucsd.edu

I. INTRODUCTION

In this paper we detail a mechanism through which matter-enhanced active-sterile neutrino transformation in the $\nu_e \rightleftharpoons \nu_s$ and $\bar{\nu}_e \rightleftharpoons \bar{\nu}_s$ channels could solve the neutron-to-seed nucleus deficit and alpha-effect problems associated with models of r -process nucleosynthesis from neutrino-heated supernova ejecta. Our solution makes the production of the r -process nuclides in neutrino-heated supernova ejecta *robust* to a wide range of uncertainties in the neutrino-driven wind models. Ultimately, our work suggests that heavy element nucleosynthesis may be a key consideration in constraining the existence of light sterile neutrinos.

By a sterile neutrino we mean one with interactions which are significantly weaker than the normal weak interaction. We demand these interactions to be weak enough so that such a sterile neutrino species would not contribute appreciably to the decay rate of the Z^0 particle. Our nucleosynthesis considerations are independent of the details of how the sterile neutrino states are constructed. For example, many models for sterile neutrinos build these species from the right-handed Dirac neutrino and left-handed Dirac antineutrino fields, leaving Majorana active neutrinos ν and Majorana sterile neutrinos N . In this case ν_s can be identified with the left-handed sterile species N_L , while $\bar{\nu}_s$ can be identified with the right-handed sterile neutrino N_R .

Of order half of the nuclei with masses $A \gtrsim 100$ were formed in the rapid neutron capture (r -process) nucleosynthesis scenario [1]. There is as yet no consensus for the site (or sites) of r -process nucleosynthesis, though it seems likely from meteoritic data-based nucleosynthesis time scale arguments that one of the sites involves the neutron-rich material associated with core collapse supernovae [2]. In turn, perhaps the most compelling model for neutron-rich material ejection following core collapse supernovae is centered on neutrino heating of material and the formation of a neutrino-driven “wind” at ~ 10 s after core bounce [3–5].

There are, however, a number of difficulties with r -process nucleosynthesis in this model. These difficulties stem principally from *astrophysical* uncertainties in the neutrino-heated outflow models. In the outflow models, r -process nucleosynthesis results from a freeze-out from nuclear statistical equilibrium. The neutrino-heated material is in the form of free nucleons near the surface of the neutron star, where its neutron-to-proton ratio (> 1) is in steady state equilibrium with the ν_e and $\bar{\nu}_e$ fluxes passing through it. As this material flows out to regions of lower temperature ($T < 700$ keV) alpha particles are formed, leaving a sea of free neutrons. Depending on the entropy per baryon, many of the alpha particles assemble into “seed” nuclei with masses between $A \approx 50$ and $A \approx 100$. As the material flows further out, to regions of even lower temperature ($T < 300$ keV), the free neutrons capture on the seed nuclei to make the r -process nuclear species.

It is clear from this picture that a key quantity for determining the outcome of the freeze-out process is the neutron to seed nucleus ratio. It is desirable to have this ratio $\gtrsim 100$ in order that the heavier r -process species (*i.e.*, those in the $A = 195$ peak) can be produced. The neutron to seed nucleus ratio is determined largely by three quantities: i) the expansion rate; ii) the neutron-to-proton ratio n/p (or, equivalently, the electron fraction $Y_e = 1/(1 + n/p)$); and iii) the entropy per baryon. Though different calculations [4,5] disagree on the value of the entropy in the neutrino-driven wind during the r -process nucleosynthesis, several models can produce values of these three parameters that yield a

high enough neutron-to-seed nucleus ratio at freeze-out to effect a reasonable r -process. Unfortunately there are neutrino-induced processes operating during or immediately after freeze-out which can work to greatly reduce the neutron-to-seed nucleus ratio to the point where acceptable r -process nucleosynthesis in this site would be impossible. These neutrino-induced r -process destroyers are: i) neutrino neutral current spallation of alpha particles; and ii) the $\nu_e + n \rightarrow p + e^-$ reaction accompanying the formation of alpha particles, also known as the “alpha effect.”

Meyer pointed out that previously neglected neutrino spallation reactions on the alpha particles tend to inhibit the r -process by allowing the assembly of too many seed nuclei [6]. This process is especially effective at wrecking the r -process where the entropy is high. A simple steady-state wind model survey of the thermodynamic parameters in neutrino-heated outflow was conducted by Qian and Woosley [7]. These authors concluded that the entropy in such models should be $\sim 100k$ per baryon, as opposed to Mayle and Wilson’s model with an entropy of $\sim 400k$ per baryon [8]. In turn, this result might argue against the effectiveness of neutrino-induced alpha particle spallation in lowering the neutron to seed nucleus ratio. However, lower entropies in general imply a lower value of this ratio since there will be more seed nuclei in these conditions. At best, the neutron to seed nucleus ratios obtained in lower entropy models are marginal for the production of the neutron-rich r -process species [9,10].

One suggested fix to the low neutron to seed nucleus ratios in these models is to invoke general relativistic effects [7,11]. These models seem attractive in that they can raise the entropy and increase the material expansion rate, both of which tend to increase the neutron to seed nucleus ratio. However, Cardall and Fuller [11] found that these models had to be finely tuned in the sense that the neutron star radius had to be close to that signaling the onset of dynamical instability. This was required, in turn, in order that the general relativistic corrections to the outflow rate and entropy be large enough to solve the neutron to seed nucleus deficit problem. However, near the dynamical instability radius the differential gravitational red-shift of ν_e and $\bar{\nu}_e$ will act to increase Y_e , partially undoing the beneficial effects of a deeper gravitational potential well [12]. The general relativistic fine tuning problem becomes even more extreme if we also demand a solution to the alpha effect problem.

The alpha effect occurs at the epoch of alpha particle formation. As the temperature drops, essentially all the protons and most of the neutrons in the ejecta lock themselves into alpha particles which have a large binding energy. This phenomenon ultimately will tend to push the electron fraction higher, towards $Y_e = 0.5$. The increase in Y_e comes about because protons produced by electron neutrino capture on neutrons will in turn capture more neutrons to bind into alpha particles, reducing the number of free neutrons available for the r -process [13]. This effect has been shown to be the biggest impediment to achieving an acceptable r -process yield [14].

One way to avoid or reduce the efficacy of the alpha effect is to reduce the flux of electron neutrinos at some point above the surface of the neutron star. However, in models of the neutrino-driven wind a large flux of electron neutrinos is required to lift the material off the surface of the neutron star. In fact since nucleons are gravitationally bound by about ~ 100 MeV near the surface of the neutron star, and since each neutrino has an energy ~ 10 MeV, each nucleon must suffer some ~ 10 neutrino interactions to be ejected to infinity. So if we are to reduce the ν_e flux we must do so only at relatively large radius, so that effective neutrino heating already can have occurred. Matter-enhanced neutrino

flavor transformation with appropriately chosen difference of the squares of the masses and vacuum mixing angles can occur above the heating region yet between the neutrinosphere and where the r -process takes place.

Ordinary active-active neutrino mixing has been extensively studied in this region of the supernova in the context of rapidly-outflowing neutrino-heated material [15–17]. These studies revealed the important interplay between the material expansion rate and the ν_e and $\bar{\nu}_e$ capture rates on free nucleons. They showed that a proper understanding of the evolution of the electron fraction Y_e in response to matter-enhanced neutrino flavor transformation could not be obtained without due consideration of the expansion rate and position of fluid elements relative to the neutrino-sphere. The inherent nonlinearity of the problem demands a coupled treatment for Y_e and the distribution of neutrino energies. Early suggestions that active-sterile neutrino transformation could be important in supernova dynamics and nucleosynthesis were made with schematic models and did not include the feedback effects of expansion [18].

Here we attempt to extend a realistic analysis of neutrino transformation with coupled outflow to the active-sterile $\nu_e \rightleftharpoons \nu_s$ and $\bar{\nu}_e \rightleftharpoons \bar{\nu}_s$ channels. The interplay of material outflow and active-sterile neutrino transformation has also been treated for a model with matter-enhanced active-active and (different) active-sterile channels by Caldwell, Fuller, and Qian [19].

The possibility of a sterile neutrino mixing with an active one was recently investigated to explain the missing neutrino fluxes in solar, atmospheric and accelerator neutrino experiments. Recent measurements of the solar neutrino flux at Superkamiokande [20] along with the earlier measurements [21] may indicate mixing of electron neutrinos with another flavor [22]. The measurement of the atmospheric electron and muon neutrino zenith angle distributions at Superkamiokande [23], taken together with the lack of observation of ν_e disappearance at the CHOOZ detector [24] present even a stronger evidence for the mixing of muon neutrinos with either tau neutrinos or sterile neutrinos [25].

Simultaneous interpretation of the solar and atmospheric neutrino deficits and the $\bar{\nu}_e$ excess observed by the LSND experiment [26] in terms of the mixing of only three active neutrinos is problematic at best [27]. These 3-neutrino fits are challenged by the observed zenith angle dependence of the atmospheric muon neutrino deficit in Superkamiokande and the establishment of an *energy dependent* solar neutrino deficit. Indeed, the only alternatives are to argue that one or more of these neutrino phenomena is unrelated to neutrino oscillation physics, or to introduce a fourth neutrino species which, because of the Z^0 -width limit, must be sterile. Some time ago it was argued that the LSND data, double beta decay and cosmological considerations suggested the necessity for introducing sterile neutrinos [28]; the recent experimental/observational data only reinforces these arguments.

In any case, *if* there really exist light sterile neutrinos probably the only way to find out about their properties is to examine astrophysical environments where neutrinos dominate the dynamics and nucleosynthesis. Matter-enhanced active-sterile neutrino transformation could have a great effect on r -process nucleosynthesis in core-collapse supernovae. We will show, in fact, that under the right conditions, such nucleosynthesis is at least as sensitive as the accelerator experiments to possible mixing of the sterile and active neutrinos.

In Section II we describe the active-sterile matter-enhancement process in the post core bounce supernova environment. In Section III we give a brief description of the supernova

outflow and nucleosynthesis model we employ, while in Section IV we outline our results. Conclusions are given in Section V.

II. MATTER-ENHANCED TRANSFORMATIONS OF ACTIVE TO STERILE NEUTRINOS

In the absence of background neutrinos the evolution of flavor eigenstates in matter is governed by the Schroedinger-like neutrino amplitude evolution equation [29]

$$i\hbar \frac{\partial}{\partial r} \begin{bmatrix} \Psi_e(r) \\ \Psi_s(r) \end{bmatrix} = \begin{bmatrix} \varphi_e(r) & \sqrt{\Lambda} \\ \sqrt{\Lambda} & -\varphi_e(r) \end{bmatrix} \begin{bmatrix} \Psi_e(r) \\ \Psi_s(r) \end{bmatrix}, \quad (2.1)$$

where

$$\varphi_e(r) = \frac{1}{4E} \left(\pm 2\sqrt{2} G_F \left[N_e^-(r) - N_e^+(r) - \frac{N_n(r)}{2} \right] E - \delta m^2 \cos 2\theta_v \right) \quad (2.2)$$

for the mixing of electron neutrinos (the plus sign on the right-hand side of the equation) or electron antineutrinos (the minus sign) with sterile neutrinos.

In these equations

$$\sqrt{\Lambda} = \frac{\delta m^2}{4E} \sin 2\theta_v, \quad (2.3)$$

$\delta m^2 \equiv m_2^2 - m_1^2$ is the vacuum mass-squared splitting, θ_v is the vacuum mixing angle, G_F is the Fermi constant, and $N_e^-(r)$, $N_e^+(r)$, and $N_n(r)$ are the number density of electrons, positrons, and neutrons respectively in the medium. Note that in what follows, we take the sterile neutrino to be predominantly the heavier mass eigenstate.

We define the potential

$$V(r) \equiv 2\sqrt{2}G_F \left[N_e^-(r) - N_e^+(r) - \frac{N_n(r)}{2} \right] \quad (2.4)$$

to be proportional to the net weak charge, such that neutrinos of energy

$$E_{\text{res}}(r) \equiv \pm \frac{\delta m^2 \cos 2\theta_v}{V(r)} \quad (2.5)$$

undergo an MSW resonance at a given positive (ν_e) or negative ($\bar{\nu}_e$) value of the potential.

The mixing of muon and tau neutrinos with sterile neutrinos may be described similarly. The evolution Hamiltonian is as for the electron neutrino species, but with φ_μ or φ_τ replacing φ_e in Eq. (2.1) as appropriate, where

$$\varphi_{\mu,\tau}(r) = -\frac{1}{4E} \left(\pm \sqrt{2} G_F N_n(r) E + \delta m^2 \cos 2\theta_v \right). \quad (2.6)$$

As before, the + sign corresponds to neutrino mixing, and the – sign to antineutrino mixing.

For a neutral medium we have $Y_p = Y_e$ and $Y_n = 1 - Y_e$, where Y_p and Y_n give the number of *all* protons or neutrons (free as well as those bound in nuclei), respectively, relative to baryons. The electron fraction Y_e is given by

$$Y_e(r) = \frac{N_e^-(r) - N_e^+(r)}{N_e^-(r) - N_e^+(r) + N_n(r)}. \quad (2.7)$$

Inserting Eq. (2.7) into Eq. (2.2) one obtains the diagonal terms in the evolution operator to be

$$\varphi_e(r) = \pm \frac{3G_F\rho(r)}{2\sqrt{2}m_N} \left(Y_e - \frac{1}{3} \right) - \frac{\delta m^2}{4E} \cos 2\theta_v, \quad (2.8)$$

and

$$\varphi_{\mu,\tau}(r) = \pm \frac{G_F\rho(r)}{2\sqrt{2}m_N} (Y_e - 1) - \frac{\delta m^2}{4E} \cos 2\theta_v, \quad (2.9)$$

where $\rho(r)$ is the matter density and m_N is the nucleon mass. Eq. (2.8) indicates that, with appropriate neutrino parameters and matter density, for $Y_e > 1/3$ only electron neutrinos and for $Y_e < 1/3$ only electron antineutrinos can undergo an active-sterile MSW resonance.

The possibility of matter-enhanced conversion of both ν_e 's and $\bar{\nu}_e$'s can have interesting consequences, but one must exercise caution. If both electron neutrino and antineutrino fluxes go through a region of neutrons and protons in equilibrium (i.e. the reactions $\nu_e + n \rightarrow p + e^-$ and $\bar{\nu}_e + p \rightarrow n + e^+$ are in steady state equilibrium with the ν_e and $\bar{\nu}_e$ fluxes), then no matter what the initial Y_e is one may naively expect that the system will evolve to a fixed point with $Y_e = 1/3$. For example, if initially $Y_e > 1/3$, the ν_e 's could transform into sterile neutrinos, greatly reducing the rate of the reaction $\nu_e + n \rightarrow p + e^-$. However, the rate of $\bar{\nu}_e + p \rightarrow n + e^+$ will remain the same, with the result that protons will be turned into neutrons, but neutrons will not be converted back to protons. Therefore, in this scenario Y_e would be driven lower. If this process brings Y_e below $1/3$, then $\bar{\nu}_e$'s could be subject to matter-enhanced conversion to sterile neutrinos. In this case, the $\bar{\nu}_e$ flux would be reduced and so an uncompensated $\nu_e + n \rightarrow p + e^-$ reaction could push Y_e above $1/3$, and so on. Indeed an earlier analysis of the resonant active to sterile conversion was given in Ref. [30] where it was argued that the electron fraction becomes stabilized in supernovae at the fixed point in the evolution, $Y_e = 1/3$, due to the feedback effects. As we will illustrate in the following sections, our realistic calculations in supernova neutrino-wind models do not bear out this assessment.

The amount of flavor conversion in an MSW resonance depends on the adiabaticity of the resonance. The adiabaticity is a function of the scale height, L_V , of the potential in Eq. (2.4):

$$L_V = \left| \left(\frac{1}{\rho} \frac{d\rho}{dr} \right) + \left(\frac{1}{Y_e - 1/3} \frac{dY_e}{dr} \right) \right|^{-1}. \quad (2.10)$$

We will refer to the scale height of the potential (or, equivalently, of weak charges) simply as “the scale height.”

A pedagogically useful approximation for the neutrino survival probability is the Landau-Zener approximation [31,32], where the survival probability is directly expressed in terms of the scale height. We emphasize that in the results presented in this paper, exact solutions of Eq. (2.2) are found numerically and the Landau-Zener approximation is not employed.

In the presence of neutrino fluxes (“background” neutrinos) the neutrino amplitude evolution Hamiltonian and the effective mass in Eq. (2.1) will have an additional term due to neutrino-neutrino neutral current forward exchange scattering. In the case of active-active neutrino evolution, the neutrino background, because of flavor mixing, contributes both diagonal and off-diagonal terms in the flavor basis amplitude evolution Hamiltonian, Eq. (2.1). However, for active-sterile mixing the off-diagonal terms are identically zero [33]. The diagonal contribution gives

$$\varphi_e(r) = \frac{G_F}{\sqrt{2}} \left[N_e^-(r) - N_e^+(r) - \frac{N_n(r)}{2} + \int d^3\mathbf{q} \left(1 - \frac{\mathbf{p}\cdot\mathbf{q}}{|\mathbf{p}||\mathbf{q}|} \right) (\rho_{\mathbf{q}} - \bar{\rho}_{\mathbf{q}})_{ee} \right] - \frac{\delta m^2}{4E} \cos 2\theta_\nu, \quad (2.11)$$

where \mathbf{p} and \mathbf{q} are the momenta of a test and a background neutrino respectively, and $(\rho_{\mathbf{q}})_{ee}$ is the matrix element of the single neutrino density matrix operator, $\langle \nu_e | \hat{\rho} | \nu_e \rangle$. Here we follow the notation and terminology of Ref. [16]. We use the net effective number of neutrinos per baryon

$$Y_\nu = \frac{m_N}{\rho} (N_\nu^{\text{eff}} - N_{\bar{\nu}}^{\text{eff}}), \quad (2.12)$$

where

$$N_\nu^{\text{eff}} \approx \frac{L_\nu}{\langle E_\nu \rangle \pi R_\nu^2} \int_0^\infty dE_{\mathbf{q}} \int d\cos\theta f_\nu(E_{\mathbf{q}}, \theta, r) (1 - \cos\alpha), \quad (2.13)$$

where $f_\nu(E_{\mathbf{q}}, \theta, r)$ is the background neutrino energy distribution function, which is obtained by evolving forward in time the initial energy distribution function,

$$f_\nu(E_\nu, \theta, r) = P(E_\nu, \theta, r) f_\nu^{\text{initial}}(E_\nu). \quad (2.14)$$

In the above, L_ν is the appropriate neutrino sphere energy luminosity of the neutrino species in question, $\langle E_\nu \rangle$ is the average energy of these background neutrinos, and $P_\nu(E_{\mathbf{q}}, r, \theta)$ is the integrated survival probability of the background neutrinos. The geometry for neutrino emission is shown in Figure 1 where the angles θ and α are defined. In our calculations we actually take the neutrino energy luminosity to originate at the center of the neutron star, but we begin the calculations of neutrino amplitude evolution only above the surface of the star (we take the surface of the neutron star to be coincident with the neutrino sphere for all species). This approximation insures the validity of the overall radial dependence of neutrino flux in the above expression. It does, however, tend to underestimate the background neutrino contribution to neutrino effective mass in the region which is very close to the neutrino sphere. In practice this is not a problem, as the matter density (the net electron density) dominates the weak potential in this region; the density scale height is so small here that neutrino flavor evolution is non-adiabatic, and so flavor transformation is suppressed. We have performed a few calculations with the luminosity originating at a neutrinosphere,

rather than at the center of the neutron star, and find that our results change very little. Finally we note that the survival probability for background neutrinos, $P_\nu(E_{\mathbf{q}}, r, \theta)$, in the above expression is “short-hand notation” for what is in actuality a complicated calculation of the evolution of the energy distribution functions for background neutrinos on various trajectories.

With the above definitions Eqs. (2.12) and (2.13) then yield

$$\varphi_e(r) = \pm \frac{G_F \rho(r)}{\sqrt{2} m_N} \left[\frac{3}{2} \left(Y_e - \frac{1}{3} \right) + \left(2Y_{\nu_e} + Y_{\nu_\mu} + Y_{\nu_\tau} \right) \right] - \frac{\delta m^2}{4E} \cos 2\theta_\nu, \quad (2.15)$$

where, as above, the positive sign in the first term gives the potential for ν_e neutrinos, while the negative sign gives that appropriate for the $\bar{\nu}_e$.

We can see from the above expressions that when $Y_e \approx 1/3$ the weak potential governing neutrino amplitude evolution will be dominated by the neutrino background. Wherever the potential is dominated by the neutrino background the problem of neutrino amplitude evolution will have an extra degree of nonlinearity. In turn, one might worry that the problem will become numerically intractable in this regime. We will argue below, however, that including a realistic material outflow scheme in this picture facilitates the numerical calculations and leads to several important features.

III. DESCRIPTION OF THE MODEL

A. General Features of Outflow

We consider outflow conditions in the supernova at several seconds post-core bounce when the r -process may take place. This late epoch in supernova evolution is easier to treat than the earlier explosion epoch (shock re-heating epoch) in several respects. It can be hoped that by this late time, well after the issue of the supernova explosion is settled, the material above the neutron star will comprise a very tenuous, nearly hydrostatic envelope. Indeed, some of the numerical simulations that can push out this far in time do tend to bear this out [4,15,34]. However, convection and other essentially multi-dimensional phenomena will undoubtedly operate. It is not completely understood *how* material from near the surface of the neutron star can be ejected to infinity. Likely any such mechanism of ejection will involve neutrino heating, which is dominated by charged-current reactions. Since each nucleon must interact with neutrinos ~ 10 times in order to be ejected from the supernova, these neutrino interactions will set Y_e in the ejecta [15]. This will be true whether or not the outflow is one-dimensional in nature or essentially involves convection and turbulent mixing. Because of this, we can obtain a fair idea of how Y_e and nucleosynthesis will change under neutrino flavor transformation by employing a simple one-dimensional outflow picture.

We choose a one dimensional neutrino-driven wind with constant expansion timescale as our hydrodynamic outflow model. Additionally, between the neutron star surface and the radius where the wind solution is appropriate, we adopt a density gradient and Y_e profile which gives a good fit to the Mayle and Wilson supernova code results. We also adopt the Mayle and Wilson calculation results for the density run in the interior of the neutron star, though we ignore feedback from neutrino physics in this region. The fitting procedure is

similar to that employed in Ref. [35]. In principle, the intermediate fit region can noticeably change the results, since the density gradient changes rapidly from very steep at the surface to very gentle in the wind. However, we have tested deviations in the fit and found that they do not change our general conclusions. Our scenarios which produce the lowest electron fractions are obtained with mixing parameters which produce non-adiabatic level crossings in the steep regions of the density gradient, with the result that neutrino conversion in such regions is suppressed or inefficient.

In the wind part of our chosen model, the outflow is naturally homologous: that is, the fluid velocity is proportional to the radial distance from the neutron star's center, $v \propto r$, where r is the radial coordinate. Simple neutrino-driven wind models are parameterized by two quantities: the assumed constant expansion timescale $\tau = r/v$, where $r = r_0 \exp(t/\tau)$; and by the entropy per baryon, S . Additionally we will assume that at sufficiently large radius the neutrino-heated ejecta will be isentropic, *i.e.* constant entropy per baryon. The relation between the density of an outgoing fluid element and the time t since it left some initial point near the neutrino sphere is $\rho \propto \rho_0 \exp(-3t/\tau)$, in the wind model. We adopt this relationship in our calculations. Clearly at very large distance from the surface of the neutron star the exponential acceleration of mass elements will no longer make sense. It has been argued, however, that this approximation will be adequate for the purposes of computing nucleosynthesis yields in the region above the neutron star before freeze-out from nuclear statistical equilibrium takes place [7]. Our calculations take place prior to this region.

A completely self consistent model to test the effects of neutrino flavor transformation may not be available for some time. However, our results indicate that the neutrino mixing solution for r -process nucleosynthesis is not finely tuned to details of the outflow model. We therefore choose representative conditions and leave it to the supernova modeling community to determine, eventually, whether such outflow and ejection mechanisms can ever be realized.

We assume that the neutrino energy luminosities, initial neutrino sphere neutrino energy spectral distributions, and the neutron star radius evolve slowly with time in comparison with the mass outflow time (time it takes for a mass element which leaves the surface of the neutron star to finish assembly of alpha particles). In fact, we can expect slow evolution of these input quantities over the duration of roughly one neutrino diffusion timescale at the epoch of r -process nucleosynthesis. Therefore we take the density/temperature gradient, Y_e profile, and neutrino flavor amplitude distributions with radius to be fixed throughout our calculations.

We employ $S_{100} = 1$ in our study, since analyses of models of the neutrino driven wind naturally pick out this entropy scale [7]. In what follows we investigate a range of dynamic expansion timescales, $\tau = 0.1 \text{ s} - 0.9 \text{ s}$. This range for τ spans the regime of plausible wind velocity for supernova models which do not include an extremely relativistic core.

From the density, entropy and electron fraction, all other thermodynamic quantities and nuclear statistical equilibrium (NSE) element abundances may be calculated by taking account of all sources of entropy in the adiabatically expanding material. This must be done without making any assumptions about whether electrons and positrons are degenerate or relativistic, since they make important contributions to the entropy.

B. Heuristic Discussion of the Neutrino-Heated Outflow

Here we give an analytic and heuristic description of neutrino-heated outflow [7]. This is meant to serve as a tool for understanding our numerical results, which, we emphasize, have been calculated without the use of many of the approximations employed in this section. One can gain qualitative insight into the general environment by noting that the neutrino physics and nucleosynthesis are qualitatively very similar to the process of Big Bang Nucleosynthesis (*e.g.*, see Ref. [40]).

In a wind model at sufficiently large radius (above the heating regime), the enthalpy per baryon is roughly the gravitational binding energy of a free baryon, or

$$TS \approx \left(\frac{M_{\text{NS}} m_b}{m_{\text{PL}}^2} \right) \frac{1}{r}, \quad (3.1)$$

where $M_{\text{NS}} \approx 1.4 M_{\odot}$ is the mass of the neutron star, m_b is the mass of a baryon (here we take it to be a proton), and the Planck mass is defined in terms of Newton's constant by $m_{\text{PL}} \equiv 1/\sqrt{G}$. With these approximations the radius (in units of 10^7 cm) at which a temperature $T_9 \equiv T/10^9$ K will be found is

$$r_7 \approx \frac{2.25}{T_9 S_{100}}, \quad (3.2)$$

where S_{100} is the entropy per baryon in units of 100 times Boltzmann's constant.

In the region above the neutron star where neutrino flavor transformation can have nucleosynthesis effects, the material will be radiation dominated and the entropy per baryon will come primarily from photons and relativistic electron/positron pairs. In this case

$$S_{100} \approx 3.339 \left(\frac{g_s}{11/2} \right) \left(\frac{T_9^3}{\rho_3} \right), \quad (3.3)$$

where g_s is the statistical weight in relativistic particles, and ρ_3 is the rest mass (baryon) density in units of 10^3 g cm^{-3} . The statistical weight in relativistic particles will be $g_s \approx 11/2$ where photons and e^{\pm} -pairs dominate, that is, when $T_9 \gtrsim 4$; and $g_s \approx 2$ for $T_9 \lesssim 4$.

An assumed constant entropy per baryon, together with the enthalpy condition in Eq. (3.1), imply that the mass density should fall off as the inverse cube of the radius. In fact, $\rho \propto S^{-4} r^{-3}$; for $M_{\text{NS}} = 1.4 M_{\odot}$,

$$\rho_3 \approx 38 \left(\frac{g_s}{11/2} \right) \frac{1}{S_{100}^4 r_7^3}. \quad (3.4)$$

For increasing values of the entropy the density scale height of the wind-envelope decreases. The density scale height of the baryon density in the wind will be

$$L_{\rho} = \left| \frac{d \ln \rho}{dr} \right|^{-1} \approx \frac{1}{3} r \approx L_{\rho 0} \left(\frac{M_{\text{NS}}}{1.4 M_{\odot}} \right) \frac{1}{T_9} \frac{1}{S_{100}} \quad (3.5)$$

where $L_{\rho 0} \approx 75.0$ km.

The effective scale height of the weak potential (*i.e.*, that relevant for determining neutrino amplitude evolution adiabaticity at a neutrino mass level crossing) will in general be

far more complicated than that in Eq. (3.5), since with cumulative neutrino transformation Y_e will *not* be a constant function of radius and the neutrino background contributions could be large, especially near neutrino mass level crossings. Just considering the weak potential stemming from neutrino forward exchange scattering on the e^\pm component of the plasma, the scale height would be,

$$L_V \approx \left| \frac{3}{r} + \frac{1}{Y_e - 1/3} \frac{dY_e}{dr} \right|^{-1}. \quad (3.6)$$

This equation would appear to imply that, for any radius, if $Y_e \approx 1/3$, then the effective scale height of weak potentials would be very small, and neutrino and antineutrino evolution through mass level crossings in these conditions would be non-adiabatic. However, for $Y_e \approx 1/3$, the weak potential will be dominated by the neutrino background and this will tend to increase the effective weak potential scale height and help facilitate adiabaticity.

The expansion rate of the material in the wind, $\lambda_{\text{exp}} \equiv 1/\tau$, is constant when we assume that the dynamic expansion timescale τ is constant. We can relate the expansion rate to the entropy per baryon and the mass outflow rate $\dot{M} = dM/dt$ [40],

$$\lambda_{\text{exp}} \equiv \frac{1}{\tau} \approx \left(\frac{45}{44\pi^2} \right) \left(\frac{11/2}{g_s} \right) N_A \left(\frac{m_{\text{PL}}^2}{M_{\text{NS}} m_b} \right)^3 S^4 \dot{M}. \quad (3.7)$$

Here $N_A = 1/m_N$ is Avogadro's number. We note that the expansion rate is extremely sensitive to the assumed entropy per baryon in the wind. Expansion timescales $\tau \sim$ a few tenths of a second, and $S_{100} \sim 1$, will imply mass outflow rates $\dot{M} \sim 10^{-6} M_\odot \text{s}^{-1}$, which are probably adequate to give an appropriate r -process ejection mass per supernova if the neutron star de-leptonization timescale is long enough.

C. Neutrino Reactions and Initial Neutrino Distribution Functions

To model the feedback effect on Y_e from expansion and the neutrino mixing process we include a numerical calculation of the reaction rates corresponding to the lepton capture processes:



In the absence of neutrino mixing, the populations of neutrinos and antineutrinos are comparable, and the forward capture process in Eq. (3.8) is not as fast as that in Eq. (3.9). This is a result of the higher average energy of the $\bar{\nu}_e$ distribution function (absent significant neutrino flavor transformation). Ultimately, it is this dominance of the rate for the forward process in Eq. (3.9) over the forward process in Eq. (3.8) which produces the neutron-rich conditions which favor the r -process. Note that the rates at large enough radius of both of the forward reactions listed above have a $1/r^2$ dependence through the neutrino flux.

We designate the rates of the reverse processes of electron and positron capture in Eq. (3.8) and Eq. (3.9) as λ_{e^-} and λ_{e^+} , respectively. At large enough radius, the forward

rates for these processes can be computed as a function of radius using ν_e or $\bar{\nu}_e$ distribution function-averaged quantities:

$$\lambda_{\nu_e}(r) \approx \left(\frac{L_{\nu_e}}{4\pi r^2} \right) \frac{1}{\langle E_{\nu_e}(r) \rangle} \langle \sigma_{\nu_e n}(r) \rangle; \quad (3.10)$$

$$\lambda_{\bar{\nu}_e}(r) \approx \left(\frac{L_{\bar{\nu}_e}}{4\pi r^2} \right) \frac{1}{\langle E_{\bar{\nu}_e}(r) \rangle} \langle \sigma_{\bar{\nu}_e p}(r) \rangle; \quad (3.11)$$

where $\sigma_{\nu_e n}$ and $\sigma_{\bar{\nu}_e p}$ are the energy-dependent cross sections for the forward processes in Eq. (3.8) and Eq. (3.9), respectively, and where angle brackets represent the appropriate neutrino (or antineutrino) distribution function averages, as in

$$\langle \sigma_{\nu_e n}(r) \rangle \equiv \int_{\Omega} \int_0^{\infty} \sigma_{\nu_e n}(E_{\nu}) f_{\nu_e}(E_{\nu}, \theta, r) dE_{\nu} d\Omega_{\nu}. \quad (3.12)$$

In the absence of neutrino conversion and for large enough radius the forward rates dominate for both process. However, the reverse rates make an important contribution when our calculations begin, even in the absence of conversion. After transformation, the forward rate or rates can be greatly reduced, increasing the importance of the back reactions. Therefore we also include positron and electron capture in our calculations.

The initial neutrino energy spectral distribution functions at the neutrino sphere are approximated here to be Fermi-Dirac. The normalized form for these *initial*, neutrino sphere energy distribution functions is then,

$$f_{\nu}^{\text{initial}}(E_{\nu}) = \frac{1}{T_{\nu}^3 F_2(\eta_{\nu})} \cdot \frac{E_{\nu}^2}{\exp(E_{\nu}/T_{\nu} - \eta_{\nu}) + 1}, \quad (3.13)$$

where E_{ν} is the neutrino (or antineutrino) energy, $\eta_{\nu} = \mu_{\nu}/T_{\nu}$ is the degeneracy parameter, or neutrino chemical potential divided by neutrino temperature T_{ν} . In Eq. (3.13) $F_2(\eta_{\nu})$ is the relativistic Fermi integral of rank two (*e.g.*, see Ref. [13], p. 795).

In fact, the true neutrino and antineutrino energy distribution functions near the neutrino sphere are revealed by detailed transport calculations [34] to in some cases deviate significantly from a Fermi-Dirac form, especially on their high energy tails. For various epochs, degeneracy parameters between $\eta_{\nu} \approx 0$ and $\eta_{\nu} \approx 3$ give the best fits to the numerical results. Here we will adopt $\eta_{\nu} = 0$ for all initial neutrino energy distributions. We take temperatures for our distributions which are typical of those obtained at 3-10 seconds post bounce, $T_{\nu_e} = 3.5$ MeV; and $T_{\bar{\nu}_e} = 4.5$ MeV. Similarly the neutrino and antineutrino energy luminosities are selected to match (roughly) those of the numerical transport calculations at this late epoch. Here we adopt $L_{\nu_e} = 1 \times 10^{51}$ ergs s⁻¹ and $L_{\bar{\nu}_e} = 1.3 \times 10^{51}$ ergs s⁻¹.

In our numerical computations of neutrino flavor mixing, we start with initial ν_e and $\bar{\nu}_e$ distribution functions at the neutrinosphere in the form given in Eq. (3.13), and zero fluxes of all sterile species. We then evolve the ν_e , $\bar{\nu}_e$, ν_s and $\bar{\nu}_s$ amplitudes so that the initial $f_{\nu}^{\text{initial}}(E_{\nu})$ evolves into the distribution functions employed in, for example, Eqs. (2.13) and (2.14): $f_{\nu}(E_{\nu}, \theta, r) = P(E_{\nu}, \theta, r) f_{\nu}^{\text{initial}}(E_{\nu})$. Note that we perform only radial evolution ($\theta = 0$) to obtain our main results. Nonradial effects are discussed at length in Section IV.

D. The Electron Fraction

The electron fraction is set by competition between the forward reactions in Eq. (3.8) and Eq. (3.9) and their reverse processes of electron and positron capture as outlined above. The rates for the latter (reverse) reactions, which depend on the electron temperature and degeneracy parameter decrease much more rapidly than the rates for the former reactions, which depend on distance from the neutron star and neutrino distribution function evolution. In the limit that the capture rates are very fast in comparison with the material expansion rate λ_{exp} in Eq. (3.7), and alpha particles are not yet present, the electron fraction reaches an equilibrium (steady state) value,

$$Y_e \rightarrow Y_{e,\text{eq}} \equiv 1/[1 + (\lambda_{\bar{\nu}_e} + \lambda_{e^-})/(\lambda_{\nu_e} + \lambda_{e^+})]. \quad (3.14)$$

Since λ_{exp} is fixed with radius, while both λ_{ν_e} and $\lambda_{\bar{\nu}_e}$ fall off with radius, there will be a point beyond which the lepton capture rates on free nucleons are very slow in comparison with the expansion rate. Beyond this point the electron fraction Y_e will assume a fixed value. In our calculations we are not in either the equilibrium (fast neutrino capture) state or the fixed (no significant capture) state. In order to accurately determine the final value of the electron fraction when alpha particles and neutrino mixing are present, we follow numerically the evolution of Y_e through the process of weak freeze out.

E. Nucleosynthesis

Here we review the evolution of a mass element which leaves the surface of the protoneutron star. Very near the neutron star surface the material is at quite a high temperature. In fact, the plasma temperature there will be comparable to the temperatures which characterize the initial ν_e and $\bar{\nu}_e$ distribution functions. In this regime NSE will obtain. At an entropy per baryon $S_{100} \sim 1$, and with the temperature this high, NSE will demand that the baryons are in free nucleons rather than nuclei, so that only neutrons and protons are present. As the material moves out to where the temperature drops below $T \lesssim 750$ keV, alpha particles begin to form.

As the fluid element moves even further out and the temperature continues to fall, it becomes energetically favorable to assemble alpha particles and free neutrons into nuclei - some heavy nuclei begin to form. At this point the material will begin to freeze out of NSE through a series of quasi-equilibrium stages [41,14]. In the freeze out from NSE the charged particle reactions fall out of equilibrium first as a result of the extreme temperature dependence of their nuclear reaction rates engendered by the large Coulomb barriers associated with big nuclei. Eventually, the only reactions left in equilibrium are neutron capture (n, γ) and photodisintegration reactions (γ, n). This final stage is when neutron capture builds the heavy nuclei which are the progenitors of the r -process nuclear species we observe in the Galaxy today.

In our calculations, along the trajectory of a fluid element we follow all thermodynamic and nuclear evolution relevant for Y_e evolution out to the point at which the first heavy nuclei begin to form. At this point Y_e has evolved to where it is essentially fixed, although a few neutrino capture reactions will still take place which can alter final element abundance

yields [14]. The nuclear equation of state which we employ in our computations is discussed at length in Ref. [35].

F. Alpha Effect

One difficulty in obtaining an adequately low electron fraction Y_e (and, hence, an adequately large neutron to seed nucleus ratio) is the alpha effect outlined in the introduction. This effect is the major impediment to obtaining a successful r -process in neutrino-driven wind models. As discussed above, as the temperature drops below a critical value which is dependent on the entropy, alpha particles begin to form. Each alpha particle removes two neutrons and two protons from the free nucleon bath. Since there were already more neutrons than protons to begin with, the ratio of free neutrons to free protons increases. This would imply that the ratio of free neutrons to free protons is larger than the n/p ratio characteristic of weak steady state equilibrium. However, on a fairly rapid timescale (just how rapid depends on the magnitudes of λ_{ν_e} and $\lambda_{\bar{\nu}_e}$), neutrino captures will occur on these free neutrons, turning them into protons. Some protons will turn to neutrons as well, but the overall ratio of free neutrons to free protons will decrease, and, hence, the overall Y_e will increase. The ultimate result of this process is that the neutron to seed nucleus ratio will decrease from what it would have been had alpha particles not formed. This is the alpha effect identified in Ref. [13].

In the alpha effect there are no compensating ν_e or $\bar{\nu}_e$ captures on alpha particles, since for the expected electron neutrino and electron antineutrino energy spectra, alpha particles are basically inert with respect to the charged current interactions. However, neutrinos and antineutrinos can still capture on nuclei and $\nu_e + n \rightarrow p + e^-$ can continue well into the neutron capture region (between $3 \gtrsim T_9 \gtrsim 1$), further robbing the r -process of its requisite neutrons [14].

Our numerical computations include a treatment of alpha particle and heavy “seed” nucleus formation as in Ref. [35]. Since we also include numerical integration of the rates in Eq. (3.10) and Eq. (3.11), our calculations will follow accurately the run-up of Y_e resulting from the alpha effect. As we will show, active-sterile neutrino transformation can result in a depressed ν_e flux relative to the no-neutrino oscillation scenario and, in turn, this can suppress the alpha effect.

IV. DISCUSSION OF RESULTS

We cast our results in terms of electron fraction Y_e at the time of the formation of heavy nuclei at $T_9 \approx 3$. This corresponds to a radius where the weak capture rates have become quite slow. Computing the evolution of the system out this far allows us to faithfully follow any potential alpha effect. Throughout the calculation, we perform a full numerical solution of the MSW evolution equations, neglecting only the effects of the neutrino background. No approximation is employed, so we can track the detailed behavior of the neutrinos as they pass through their resonances. In understanding the results, however, it will be useful to keep in mind the dependence of survival probability on scale height. In our scenario, where neutrino evolution begins at very large potentials and the vacuum mixing angle is small,

passage through an adiabatic resonance (with a large scale height) gives near-complete conversion; passage through a non-adiabatic resonance (with a small scale height) yields very little conversion.

We couple the MSW evolution to a numerical calculation which self consistently determines temperature, electron chemical potential and nuclear statistical equilibrium abundances of protons, neutrons, and alpha particles, from the entropy, density and electron fraction at each time step. Also at each time step, all weak capture rates are calculated, using the survival probabilities for each neutrino and antineutrino energy bin, and the electron fraction Y_e is updated. This new Y_e is then used to determine the new neutrino survival probabilities, as well as the updated thermodynamic and abundance variables. Implementation of this feedback effect is the substantially new element in our approach to neutrino transformations in supernovae. At very high densities, the electron fraction is set primarily by degeneracy. Its increase before $\rho = 10^8$ g/cm³ is controlled initially by neutrino capture on neutrons, Eq. (3.9). As the degeneracy is lifted, positron capture on neutrons further raises and contributes quite significantly to the electron fraction. Thus, because of the importance of positron and electron capture at small radius, we expect feedback effects to be small in the region where we use a static profile of Y_e . For the highest densities ($\rho > 4 \times 10^8$ g/cm³), then, we use a static electron fraction profile to compute the MSW evolution of the neutrino amplitudes.

A. The Mechanism

In this section we describe the numerical evolution of neutrinos and antineutrinos in concert with the composition and the Y_e value of outflowing mass elements. We focus on the feedback mechanism: roughly (neglecting the neutrino background terms) the value of Y_e determines whether neutrino flavor transformation takes place, while ν_e and $\bar{\nu}_e$ captures determine Y_e .

Here we do not follow the evolution of the ν_μ , $\bar{\nu}_\mu$, ν_τ , and $\bar{\nu}_\tau$ distribution functions. However, depending on the adopted neutrino mass level schemes, there could well be transformations either among these species or with ν_e 's, or even with sterile neutrino species. The possible effects of some of these types of neutrino transformation channels are treated elsewhere [19]. In principle neutrino transformation among the mu and tau neutrinos and sterile species could affect the neutrino background which is partly responsible for driving ν_e and $\bar{\nu}_e$ evolution.

We find that neutrino background effects are everywhere sub-dominant, except very close to where $Y_e = 1/3$. The neutrino background in principle can change both the position of the resonance and the scale height. (Recall that “the scale height” is the scale height of weak potential.) However, since the density gradient is so steep, the small contribution from the background has little impact on the resonance position.

For large neutrino energies, the scale height at resonance is dominated by the derivative of Y_e near 1/3 before we introduce background effects. The neutrino background may significantly change the conversion probability for those neutrinos. This change affects neutrinos of much higher energy than the ones we consider, and so we neglect the background in the following discussion. For example, we estimate that background makes an unimportant contribution to the scale height for neutrinos below 50 MeV as long as $\delta m^2 \gtrsim 0.1$. We will

consider the effects of including neutrino background in more detail after the discussion of the main result.

The potential for electron neutrino and electron antineutrino active-sterile transformation is controlled by density and electron fraction, since the potential $V \propto \rho(Y_e - 1/3)$. When the potential is positive, the $\nu_e \rightleftharpoons \nu_s$ channel operates, and when the potential is negative, the $\bar{\nu}_e \rightleftharpoons \bar{\nu}_s$ transformation can take place.

At the surface of the protoneutron star the density profile is very steeply falling, while the electron fraction Y_e is rising, as can be seen in Figures 2 and 3. Since $Y_e < 1/3$ very near the neutron star surface, there is an initial resonance for $\bar{\nu}_e \rightleftharpoons \bar{\nu}_s$ at high density, $\rho = 2 - 3 \times 10^9 \text{ g cm}^{-3}$. Immediately following this antineutrino resonance is an electron neutrino resonance ($\nu_e \rightleftharpoons \nu_s$), as Y_e passes above $1/3$. In this region, the density profile is steep; Y_e is changing rapidly with radius; and $Y_e \approx 1/3$. Therefore, the scale height is tiny (see Eq. 2.10), so these resonances are usually quite nonadiabatic and do not yield significant flavor transformation. At very large $\delta m^2 \sin^2 2\theta$, the resonances may become adiabatic. We will return to this point below.

For regions above the protoneutron star where $T_9 \lesssim 25$, the outflow goes over to the neutrino-driven wind solution with constant dynamic expansion timescale, and we begin to include feedback effects in our calculation. In the wind the density continues to fall with increasing distance, although much less steeply than at the surface as can be seen from Eq. (3.5). In this region Y_e roughly levels off with radius (before neutrino mixing effects), and the falling density allows the electron neutrinos to pass through a resonance. The density gradient is much smaller here, and so this resonance is likely to result in more adiabatic flavor transformation, for a wide range of neutrino mixing parameters and for a broad range of neutrino energies.

This transformation is visible in Figure 4, where we show the electron neutrino capture rate on neutrons as a function of radius (with the $1/r^2$ dependence of the neutrino flux divided out). Since we begin at high density, and therefore large weak potential, low-energy ν_e 's transform to sterile neutrinos first. As the potential falls with density, higher energy ν_e 's transform.

For a sufficiently long dynamical expansion timescale (small λ_{exp}) as in this example, the plummeting ν_e capture rate, λ_{ν_e} , eventually falls well below $\lambda_{\bar{\nu}_e}$. This unbalances the weak steady state equilibrium and tends to shift it in favor of the reaction $\bar{\nu}_e + p \rightarrow n + e^+$. Therefore Y_e is driven down, as can be seen in Figure 3. This figure shows both the equilibrium electron fraction (Eq. 3.14) and the actual electron fraction. The local minimum in the equilibrium electron fraction occurs when the ν_e 's disappear. The equilibrium Y_e is not driven all the way to zero at this point, since positron capture on neutrons is still marginally significant.

A decreasing Y_e causes $V(r)$ to decrease more quickly than would be the case were Y_e to remain fixed. This behavior can be seen in Figure 5. Another consequence of the rapid decrease in Y_e is that the scale height becomes smaller (see Eq. 3.6) and neutrino amplitude evolution through the $\nu_e \rightleftharpoons \nu_s$ resonances becomes somewhat less adiabatic. Conversion of high-energy electron neutrinos, then, is slightly less efficient than conversion of low-energy neutrinos. However, for a large range of neutrino mixing parameters, almost all electron neutrinos transform into sterile states.

More importantly, the disappearance of the ν_e 's can push the electron fraction to values

$Y_e < 1/3$, making V negative. As a result, high energy $\bar{\nu}_e$'s will undergo a resonance and convert to $\bar{\nu}_s$'s. This does not usually drive Y_e back up, since there are so few ν_e 's left. However, it slows down the fall of Y_e with radius, creating a “knee” in the actual electron fraction curve at around 14 km in Figure 3.

The beginning of the return of the electron antineutrinos is marked by the local maximum in Y_e . When Y_e is near $1/3$, the change in the weak potential is dominated by the change in the electron fraction. However, when Y_e is far from $1/3$, the change in the potential is dominated by the change in the density, which is falling rapidly. This tends to pull the potential toward zero, turning it over and preventing lower-energy $\bar{\nu}_e$'s from transforming and causing the higher energy $\bar{\nu}_s$'s, which resulted from $\bar{\nu}_e \rightarrow \bar{\nu}_s$, to transform back to active states. This regeneration of $\bar{\nu}_e$'s results in the recovery of nearly their full population (Figure 4). Along with the decreasing importance of positron capture, the regeneration of the $\bar{\nu}_e$'s allows the electron fraction to fall to very low values. Figure 6 shows explicitly the energy of the ν_e 's and $\bar{\nu}_e$'s which undergo a resonance at a given position.

In our calculations, the choice of the dynamic expansion timescale plays a crucial role in determining the final electron fraction. With a relatively long timescale (as in our example), many neutrino and antineutrino captures are possible, and the actual Y_e closely tracks the equilibrium Y_e . A longer dynamic expansion timescale also augments the alpha effect if many ν_e 's are still present. In Figure 3, a small alpha effect can be seen as the upturn in Y_e at around 25 km.

B. Variation of Parameters

Figure 7 explores the effect of variation in the neutrino mixing parameters. Here we plot the value of Y_e , just as alpha particle formation is ending and heavy nucleus formation is beginning, for a wind model with a dynamical expansion timescale of $\tau = 0.3$ s. One indication of whether r -process nucleosynthesis may successfully occur is if the neutron to seed nucleus ratio (R) at the time rapid neutron capture begins is around 100. If R is considerably smaller than 100, then the $A=195$ peak will not form. According to Meyer and Brown [10], for a dynamic expansion timescale of 0.3 seconds $R > 100$ is possible if $Y_e < 0.18$. (Note that the definition of our timescales differs; ours is three times theirs.) The $Y_e = 0.18$ contour is shown as the dotted line in Figure 7. As mentioned above, there can be further change in the electron fraction during the first stages of heavy nucleus formation (after our calculation ends). However, if the electron neutrino survival probability is small, we expect this change to be minimal.

The electron fraction is larger than is desirable for r -process nucleosynthesis on both the upper right and lower left sides of the figure. We compare these regions to the optimal behavior (center of the figure) which was described in detail above. As $\delta m^2 \sin^2 2\theta$ decreases, conversion of electron neutrinos is less effective, since evolution through the resonances becomes less adiabatic. In the lower left corner of the plot, it can be seen that Y_e is asymptotically approaching the value it takes on without neutrino mixing.

As $\delta m^2 \sin^2 2\theta$ increases, it becomes possible to have flavor transformation proceed through the resonances which are closest to the neutron star surface. This can result in some of the electron neutrinos and antineutrinos being partially converted to sterile species before they leave the vicinity of the surface of the protoneutron star. When the ν_e 's en-

counter the later resonances, those that were previously converted to steriles can convert back to electron neutrinos. This leaves a partial complement of electron neutrinos which causes Y_e to drop less than in our optimal example.

When $\delta m^2 \sin^2 2\theta$ is large, most ν_e 's and $\bar{\nu}_e$'s convert to sterile states in the inner resonances. Then, in the wind region, ν_s 's convert back to active states and the ν_e 's convert to sterile states. For sufficiently large $\delta m^2 \sin^2 2\theta$, we end up with a large population of active ν_e 's and a smaller population of $\bar{\nu}_e$'s. This drives the electron fraction above 0.5 and the later $\bar{\nu}_e$ mass level crossings never occur.

In this region nonradial neutrino paths play an important role in the neutrino evolution. Neutrinos which leave the neutrino sphere nonradially find the inner resonances more adiabatic, since they encounter them at a grazing angle. Therefore, if we consider nonradial neutrino paths, the inmost resonance will begin to cause transformation at lower $\delta m^2 \sin^2 2\theta$. We do not include these effects in Figure 7, but we estimate their importance by computing the relative difference in the ν_e capture rate on neutrons at 11 km with and without nonradial effects:

$$\text{relative difference} = \frac{(\text{radial rate}) - (\text{nonradial rate})}{(\text{nonradial rate})}. \quad (4.1)$$

(As can be guessed readily from the neutrino emission geometry, nonradial neutrino paths have very little effect at larger radii.) The relative difference is shown in Figure 10. The dotted line in Figure 7 corresponds to a 10% reduction in the ν_e capture rate from nonradial effects. Above this line, a full treatment of neutrino oscillations in the presence of neutrino scattering at high density, including nonradial effects would be necessary in order to fully understand the implications of these neutrino mixing parameters for r -process nucleosynthesis.

Although the lines of constant $\delta m^2 \sin^2 2\theta$ describe much of the behavior seen in the plot, there is additional variation above and below the island of lowest electron fraction. As δm^2 decreases along a line of constant $\delta m^2 \sin^2 2\theta$, the density at which the electron neutrino resonance occurs decreases and the distance from the protoneutron star increases. At larger distance the neutrino capture rates are smaller, due to the $1/r^2$ dependence in the neutrino fluxes, so the actual Y_e approaches the equilibrium Y_e more slowly. Therefore, the final Y_e is higher. On the other hand, as δm^2 increases, the electron neutrinos convert at higher density, where the scale height is smaller, and therefore ν_e conversion is less efficient. The ν_e 's which survive conversion in this case cause a larger alpha effect.

In Figures 8 and 9, we investigate the impact of varying the dynamic expansion timescale. With a longer timescale (Figure 9), there is more time for the actual Y_e to approach the equilibrium value, but also a stronger alpha effect. The alpha effect pulls the final electron fraction toward 0.5, shifting all the contours away from the 0.5 contour, as compared with the shorter expansion timescale case.

We will now consider the movement of the island of smallest Y_e as the dynamic expansion timescale varies. The island moves up and down in δm^2 , roughly along lines of constant $\delta m^2 \sin^2 2\theta$. There is a different location for the optimal island of parameter space because different resonance locations are optimal in reducing Y_e for different dynamic expansion timescales.

There are three ways that the resonance location affects the final value of Y_e . First, the closer the neutrino mass level crossing position is to the surface of the protoneutron star, the

more readily the actual value of Y_e will track the equilibrium value. This is mostly because of the $1/r^2$ dependence of the neutrino flux and the associated radial dependence of λ_{ν_e} and $\lambda_{\bar{\nu}_e}$. Second, the resonance position—and thus its adiabaticity—affects the number of ν_e 's present when alpha particles form, and therefore partly determines the strength of the alpha effect. Finally, the two $\bar{\nu}_e$ resonances in the wind region may have different adiabaticities.

For the very short ranges of dynamic expansion timescale, the optimal island in parameter space moves to larger values of δm^2 , where the resonances are closer in general to the surface of the neutron star. A deep resonance produces the lowest Y_e at short expansion timescale primarily because it is necessary to convert the ν_e 's where the neutrino fluxes are large, so that the actual value of Y_e tracks its equilibrium value. At short expansion timescale the electron fraction falls out of weak equilibrium quickly. Since a deep resonance is less adiabatic, it leaves a larger population of residual ν_e 's when alpha particles form. However, at short dynamic expansion timescale, the alpha effect can be quite small, so that the surviving ν_e 's have little effect. Since the electron fraction freezes out so quickly at short dynamic expansion timescale (the weak freeze out radius is small in this case), the population of $\bar{\nu}_e$'s becomes relatively unimportant by the time they begin to convert to sterile species.

Conversely, at long dynamic expansion timescale, the island of optimal parameter space for reducing Y_e moves to smaller values of δm^2 . The resonances in this case are farther from the surface of the neutron star. Here it is not so important to convert the ν_e 's deep in the supernova, because in this scenario there will be time for them to affect the electron fraction even if their flux is relatively small.

It is, however, important to convert as many ν_e 's as possible in this case, if the pernicious increase in Y_e stemming from the alpha effect is to be minimized. Finally, for this scenario, the population of $\bar{\nu}_e$'s at larger radius will be important, since the actual electron fraction does track its equilibrium value so closely. As the ν_e 's convert to sterile species, the actual electron fraction falls very quickly through $1/3$, and $\bar{\nu}_e$'s begin to convert to steriles. Both because Y_e is falling so quickly and because this first $\bar{\nu}_e$ resonance occurs at a position where there is a comparatively large density gradient, the neutrino amplitude evolution through the resonance may not be completely adiabatic. The second $\bar{\nu}_e$ resonance, however, will be adiabatic as usual. Thus, some $\bar{\nu}_e$'s will not convert in the first resonance, but will convert to steriles in the second. The net effect is to lower the population of $\bar{\nu}_e$'s, and therefore raise the equilibrium value of Y_e . This effect is minimized if the resonances occur far from the surface of the neutron star, where they are largely adiabatic.

In both the $\tau = 0.1$ s and $\tau = 0.9$ s cases, the minimum in final Y_e is larger than the minimum in the $\tau = 0.3$ s case. In the limit of very short dynamic expansion timescale, the number of neutrino captures after the ν_e resonance is very small and the electron fraction remains high. For example at $\tau = 0.01$ s, neutrino conversion has very little effect on the electron fraction. The region of low Y_e will disappear at very low expansion rate, owing to the strengthening of the alpha effect in this limit.

An alternative solution to the r -process problem would be to invoke a very rapid outflow in the absence of neutrino flavor transformation. This suppresses both the alpha effect and the assembly of seed nuclei, therefore increasing the neutron-to-seed ratio. However, it is not obvious that the neutrino heating mechanism can be responsible for such rapid ejection.

In addition to the variation of parameters in the wind model, one must also consider variation in the density profile before the wind takes over. This is particularly important

since if this is less steep than in our example, there will be more conversion of electron neutrinos in the first resonance, potentially destroying the low Y_e solution that we have presented. We tested this by employing a different, unrealistically flat density gradient in the intermediate region, the potential for which is shown in Figure 11, and generating the same type of contour plot as in our main example. The results are shown in Figure 12. Clearly, this part of the density profile has a quantitative impact on the solution, although it does not change our qualitative conclusions.

V. CONCLUSIONS

Here we have followed in the region above a hot protoneutron star the evolution of the ν_e and $\bar{\nu}_e$ neutrino distribution functions including active-sterile neutrino transformation in the channels $\nu_e \rightleftharpoons \nu_s$ and $\bar{\nu}_e \rightleftharpoons \bar{\nu}_s$. This evolution was calculated from the surface of the neutron star through the region in which the key input quantities for r -process nucleosynthesis are determined. We employed a realistic outflow model which included feedback effects from material expansion and neutrino flavor/type evolution and which included a nuclear equation of state sophisticated enough to model adequately the alpha effect.

We have found that a very interesting range of vacuum neutrino mass-squared differences $3\text{ eV}^2 \lesssim \delta m_{\text{es}}^2 \lesssim q70\text{ eV}^2$ and vacuum mixing angles $\sin^2 2\theta_{\text{es}} \gtrsim 10^{-3}$ produces effects which favor an increase in the neutron to seed nucleus ratio. (Here, δm_{es}^2 and θ_{es} refer to the parameters that control the $\nu_e \rightleftharpoons \nu_s$ and $\bar{\nu}_e \rightleftharpoons \bar{\nu}_s$ evolution.) In fact, the optimal range in neutrino mixing parameters produces a greatly reduced electron fraction Y_e and a significantly smaller population of ν_e 's irradiating the nucleosynthesis region. These effects act to aid r -process nucleosynthesis in two ways: (1) the lower Y_e translates directly into more neutrons that can be captured to make the heavy r -process nuclides; and (2), the diminished flux of ν_e 's helps to disable the pernicious alpha effect, which is a serious obstacle to obtaining r -process nucleosynthesis in neutrino-heated supernova ejecta.

These effects that are beneficial to the r -process in this site come about through the disproportionate disappearance of the ν_e population relative to the $\bar{\nu}_e$'s. In turn, the reason that so many more ν_e 's are converted to sterile species than $\bar{\nu}_e \rightarrow \bar{\nu}_s$ in our calculation has to do with a new effect which we point out here for the first time. A self consistent calculation of the electron fraction Y_e with neutrino transformation and with a proper treatment of the material outflow rate shows that although the $\bar{\nu}_e$ are converted to sterile species, they are re-generated before the Y_e in the wind freezes out. This behavior also prevents the system from reaching the fixed point in its evolution, $Y_e = 1/3$.

A proper treatment of expansion coupled with Y_e evolution is a necessary step in obtaining this new result. In fact, we find that the weak potential driving $\bar{\nu}_e \rightleftharpoons \bar{\nu}_s$ immediately past the radius where Y_e crosses below $1/3$ has a peaked structure with radius. This potential at first rises as the quantity $(1/3 - Y_e)$ rises, and then falls with increasing radius as the baryon density drops. This implies that there will be two level crossings (resonances) in the $\bar{\nu}_e \rightleftharpoons \bar{\nu}_s$ channel within a short space in radius. Therefore $\bar{\nu}_e$'s converted at the first resonance are re-generated at the second.

We have employed several approximations in obtaining this result, some of which we are pursuing with further investigation. For convenience in computation, we have treated the neutrino flux as arising from a point source. This is unphysical on several grounds: it

leads to a too rapid fall-off with radius of neutrino and antineutrino capture rates; and it implies no neutrino background terms in the weak potential. As outlined above, however, we expect the neutrino background to dominate the weak potential where $Y_e \approx 1/3$. Just where and to what extent the background will dominate and alter the neutrino flavor evolution from what we have presented here depends on the neutrino energy spectra and luminosities. In turn, there exists a wide range of possible values for these quantities at the late epoch where r -process nucleosynthesis is an issue. This variation in neutrino emission parameters reflects the range of nuclear equations of state, neutrino opacities, and neutrino transport physics employed in the various numerical computations. We are investigating the ranges of late-time supernova conditions for which our effect will be operative.

We have implicitly assumed here that the de-leptonizing neutron star is not itself a source of sterile neutrinos. This seems reasonable on two grounds. First, we can invoke very small vacuum mixing angles between active and sterile neutrino species. That suits our purposes in the late-time neutrino-driven wind because we rely on matter-enhancement of neutrino flavor transformation. For the neutrino mass differences employed in this paper there will be no mass level crossings deep in the core and, in fact, matter effects will then further suppress mixing. Second, the neutrino mean free paths in the core can be very short, so that coherent flavor transformation is unlikely. The problem of neutrino production, interaction, and propagation in dense and hot nuclear matter is a difficult one and merits much further study.

Of course, it is never legitimate to invoke novel weak interaction physics at some point late in the evolution of the supernova without an assessment of how this new physics could have altered the picture in earlier epochs. In particular, what would be the effects of the neutrino mass and mixing scheme we invoke here to help the r -process on the core infall epoch, and on the shock re-heating epoch? The infall of the pre-supernova iron core is characterized by low entropy per baryon, relatively high densities ($\rho \gtrsim 10^{11} \text{ g cm}^{-3}$ where neutrinos are trapped and at least partially thermalized) and, with the typical equations of state employed, electron fractions $Y_e > 1/3$. These conditions imply that our chosen range of neutrino mass and mixing parameters will produce no neutrino mass level crossings which could alter the standard core collapse picture. In short, the required δm^2 to obtain a level crossing on infall is much larger (see Ref. [36]).

Likewise, the δm^2 values required to obtain a neutrino mass level crossing under the shock during the supernova explosion (or shock re-heating) epoch are large $\delta m^2 \gtrsim 100 \text{ eV}^2$ (see Ref. [37] for a discussion of active-active neutrino flavor transformation during shock re-heating). At this epoch, however, we are much less certain about the range of Y_e values likely to be encountered either near the surface of the core or in the higher entropy material behind the shock.

In fact, we expect this epoch to be accompanied by salt-finger-like convective instability through the neutrino sphere, which could greatly increase the neutrino luminosities and neutrino heating rates immediately above the hot proto-neutron star surface. In turn, this increased heating probably leads to convection and to large and small scale inhomogeneities in density, entropy, and electron fraction. It is possible that the fluctuation amplitudes on relevant scales at this epoch will be large enough to destroy complete adiabatic neutrino flavor evolution through resonances and, hence, render our scheme inoperative at these early times. Note, however, that it may be reasonable to assume that the material

outflow is much smoother and so conducive to adiabatic neutrino flavor evolution in the later neutrino-driven outflow regime where we envision the r -process to originate and where our scheme could operate. Fluctuation-induced neutrino flavor de-polarization in the context of supernovae and the sun has been investigated in detail in the active-active channel [38], and these studies should be directly applicable as well in the active-sterile channel employed here.

We intend to investigate the effects of active-sterile mixing schemes on shock re-heating and on the production of the neutron number $N=50$ nuclei and the light p -nuclei which may originate during this epoch [13,39]. In particular, if large scale neutrino flavor transformation somehow *does* occur at this epoch, then a reduction in the electron fraction would exacerbate the existing problem in some supernova models of the overproduction of $N=50$ nuclei. Ultimately, since the conditions during the shock re-heating epoch and the later neutrino-driven wind epoch are so disparate, we feel that our new scheme to help the r -process stands on its own.

Our results are potentially significant in the debate over *where* r -process nucleosynthesis takes place in the Galaxy. There is fair evidence that at least some of the r -process nuclides are made in an environment associated with core collapse supernovae (Type II, Type Ib and Ic supernovae) [2].

As outlined above, it is so far difficult to obtain conditions favorable for r -process nucleosynthesis in conventional neutrino-driven outflow models [14], especially when the alpha effect is included [13]. It is an open question as to whether or not the problems with r -process nucleosynthesis in this site can be remedied through the tuning of the astrophysical aspects of the outflow model. Furthermore, it is not really known whether it is *required* to have r -process nucleosynthesis come from this site in order to explain the observational and meteoritic data (see Ref. [40]). It has been argued, however, that neutrino post-processing may be important in understanding the observed abundance patterns and this may imply that supernovae or neutron star binary mergers, or both, play a role in r -process synthesis [42].

Based on our work here we can say, however, that if neutrino mass and mixing parameters are in our optimal range, then a broad class of neutrino-driven outflow models have the *necessary* conditions to produce the r -process. Moreover, we would obtain the r -process in these models in a way which was robust to the details and astrophysical uncertainties in the models over a fairly broad range of outflow parameters. The issue of *sufficiency* of r -process nucleosynthesis in this case is another matter and could only be answered with a detailed nuclear reaction network which included neutron capture and photo-disintegration all coupled with a consistent hydrodynamic calculation, as well as all of our neutrino physics effects.

So, does the existence of r -process nuclides in the abundances measured in the Sun and other stars and with the synthesis rates inferred in the Galaxy then imply the existence of light sterile neutrinos? The answer is no, since we cannot at this time preclude other non-neutrino-mixing astrophysical fixes for the r -process, and we cannot say for absolutely certain that we need the r -process from neutrino-heated supernova ejecta. Nevertheless, it is interesting that light sterile neutrinos mixing with electron neutrinos could affect the synthesis of the heaviest elements. At the present time there is a flurry of new instruments which are bringing in new data which bears on the issues surrounding r -process nucleosynthesis, so

it may be possible in the future to resolve uncertainties. If there truly are “sterile” neutrinos, then astrophysical means, principally nucleosynthetic, represent probably our only hope for learning about their properties.

Finally, what of the implications of our results for particle physics? In our models we ignore the mu and tau neutrinos and their anti-particles as these play a negligible role in the nucleosynthesis scenario considered here. Our model would, for example, be consistent with having the sterile neutrino mass at around $\sim 2 - 8$ eV while having all of the active neutrinos clustered near zero mass, with the ν_e and ν_μ/ν_τ split by $\sim 10^{-10}$ eV² to $\sim 10^{-4}$ eV² to give the favored solar neutrino solutions, and to have the mu and tau neutrino maximally mixed with their masses split by some $\sim 10^{-2}$ eV² to give the Superkamiokande result for atmospheric neutrinos. The LSND result could be accommodated in our model by invoking an indirect vacuum oscillation of $\bar{\nu}_\mu$ into $\bar{\nu}_e$ via the sterile species, $\bar{\nu}_\mu \rightarrow \bar{\nu}_s \rightarrow \bar{\nu}_e$ [43]. By contrast, other schemes involving sterile neutrinos designed to fix the r -process [19], would predict active-sterile mixing in the sun as a solution of the solar neutrino problem. We may have a resolution of this question from the Sudbury Neutrino Observatory in the near future. In any case, the future is promising for the role of r -process studies to help constrain neutrino mass and mixing models. In turn, future neutrino oscillation experiments conceivably could help us to constrain the site of r -process nucleosynthesis.

ACKNOWLEDGMENTS

This work was supported in part by the U.S. National Science Foundation Grants No. PHY-9605140 at the University of Wisconsin, and PHY-9800980 at the University of California, San Diego, and in part by the University of Wisconsin Research Committee with funds granted by the Wisconsin Alumni Research Foundation. We thank the Institute for Nuclear Theory and Department of Astronomy at the University of Washington, and Aspen Center for Physics for their hospitality and Department of Energy for partial support during the completion of this work.

REFERENCES

- [1] E.M. Burbidge, G.R. Burbidge, W.A. Fowler, and F. Hoyle, *Rev. Mod. Phys.* **29**, 547 (1957); A. G. W. Cameron, *Proc. Astron. Soc. Pacific* **69**, 201 (1957).
- [2] Y.-Z. Qian, P. Vogel, and G. J. Wasserburg, *Astrophys. J.* **494**, 285 (1998).
- [3] S.E. Woosley and R.D. Hoffman, *Astrophys. J.* **395**, 202 (1992).
- [4] S.E. Woosley, J.R. Wilson, G.J. Mathews, R.D. Hoffman, and B.S. Meyer, *Astrophys. J.* **433**, 229 (1994); B.S. Meyer, W.M. Howard, G.J. Mathews, S.E. Woosley, and R.D. Hoffman, *Astrophys. J.* **399**, 656 (1992).
- [5] K. Takahashi, J. Witt, and H.-Th. Janka, *Astron. Astrophys.* **286**, 857 (1994).
- [6] B.S. Meyer, *Astrophys. J.*, **449**, L55 (1995).
- [7] Y.-Z. Qian and S.E. Woosley, *Astrophys. J.*, **471**, 331 (1996).
- [8] J.R. Wilson, as quoted in Ref. [4].
- [9] R. D. Hoffman, S. E. Woosley, and Y.-Z. Qian, *Astrophys. J.* **482**, 951 (1996).
- [10] B. S. Meyer and J. S. Brown, *Astrophys. J. Suppl.* **112**, 199 (1997).
- [11] C. Y. Cardall and G. M. Fuller, *Astrophys. J. Lett.* **486**, L111 (1997).
- [12] G. M. Fuller and Y.-Z. Qian, *Nucl. Phys. A* **606**, 167 (1996).
- [13] G.M. Fuller and B.S. Meyer, *Astrophys. J.*, **453**, 792 (1995).
- [14] B. S. Meyer, G. C. McLaughlin, and G. M. Fuller, *Phys. Rev. C*, *in press* (1998).
- [15] Y.-Z. Qian, *et al.*, *Phys. Rev. Lett.* **71**, 1965 (1993).
- [16] Y.-Z. Qian and G.M. Fuller, *Phys. Rev. D* **51**, 1479 (1995), **52**, 656 (1995).
- [17] G. Sigl, *Phys. Rev. D* **51**, 4035 (1995).
- [18] J. T. Peltoniemi, *Astron. Astrophys.*, **254**, 121 (1992); J. T. Peltoniemi, preprint hep-ph/9511323, unpublished (1995).
- [19] D. O. Caldwell, G. M. Fuller, and Y.-Z. Qian, *Phys. Rev. D*, *submitted* (1998).
- [20] Y. Fukuda, *et al.*, (The Superkamiokande collaboration), *Phys. Rev. Lett.* **81**, 1158 (1998).
- [21] B.T. Cleveland, T. Daily, R. Davis, J.R. Distel, K. Lande, C.K. Lee, P.S. Wildenhain, and J. Ullman, *Astrophys. J.* **496**, 505 (1998); W. Hampel, *et al.* (GALLEX Collaboration), *Phys. Lett. B* **388**, 384 (1996), **420**, 114 (1998), *ibid.* **436**, 158 (1998); J.N. Abdurashitov, *et al.* (SAGE Collaboration), *Nucl. Phys. Proc. Suppl.* **48**, 299 (1996), hep-ph/9803418.
- [22] J.N. Bahcall, P.I. Krastev, and A.Yu. Smirnov, *Phys. Rev. D* **58**, 096016 (1998); V. Barger, S. Pakvasa, T. J. Weiler, and K. Whisnant, *ibid.*, 093016 (1998); N. Hata and P. Langacker, *ibid* **56**, 6107 (1997).
- [23] Y. Fukuda, *et al.*, (The Superkamiokande collaboration), *Phys. Rev. Lett.* **81**, 1562 (1998); *Phys. Lett. B* **436**, 33 (1998).
- [24] M. Apollonio, *et al.* (The CHOOZ collaboration), *Phys. Lett. B* **420**, 397 (1998).
- [25] M. Fukugita, M. Tanimoto, and T. Yanagida, *Phys. Rev. D* **57**, 4429 (1998); R. Foot, R. R. Volkas, and O. Yasuda, *Phys. Rev. D* **58**, 013006 (1998); Q.Y. Liu and A.Yu. Smirnov, *Nucl. Phys. B* **524**, 505 (1998); G.L. Fogli, E. Lisi, A. Marrone, and D. Montanino, *Phys. Lett. B* **425**, 341 (1998); M. C. Gonzalez-Garcia, H. Nunokawa, O. L. G. Peres, T. Stanev, and J. W. F. Valle, *Phys. Rev. D* **58**, 033004 (1998); P. Lipari and M. Lusignoli, *Phys. Rev. D* **58** 073005 (1998); M. C. Gonzalez-Garcia, H. Nunokawa, O. L. G. Peres, and J. W. F. Valle, hep-ph/9807305. V. Barger, T. J. Weiler, and K.

- Whisnant, Phys. Lett. B **440**, 1 (1998); G.L. Fogli, E. Lisi, A. Marrone, and G. Scioscia, Phys. Rev. D **59**, 033001 (1999).
- [26] C. Athanassopoulos, *et al.* (LSND Collaboration), Phys. Rev. Lett. **75**, 2650 (1996), **77**, 3082 (1996), Phys. Rev. C **54**, 2685 (1996), Phys. Rev. C **58**, 2489 (1998); see also J.E. Hill, Phys. Rev. Lett. **75**, 2654 (1996).
- [27] C. Y. Cardall and G. M. Fuller, Phys. Rev. D**53**, 4421 (1996); G. L. Fogli, E. Lisi, and G. Scioscia, Phys. Rev. D**52**, 5334 (1995); A. Acker and S. Pakvasa, Phys. Lett. **B397**, 209 (1997); P. Harrison, D. Perkins, and W.Scott, Phys. Rev. **B349**, 137 (1995); R. P. Thun and S. Mckee, Phys. Lett. B **439**, 123 (1998); V. Barger, T. J. Weiler, and K. Whisnant, Phys. Lett. B **440**, 1 (1998); T. Teshima and T. Sakai hep-ph/9805386 and hep-ph/9801276.
- [28] D. O. Caldwell and R. N. Mohapatra, Phys. Rev. D**48**, 3259 (1993); D. O. Caldwell and R. N. Mohapatra, Phys. Lett. B **354**, 371 (1995); G. M. Fuller, J. R. Primack, and Y.-Z. Qian, Phys. Rev. D**52**, 1288 (1995).
- [29] S.P. Mikheyev and A. Yu. Smirnov, Sov. J. Nucl. Phys. **42**, 913 (1985); Sov. Phys. JETP **64**, 4 (1986); L. Wolfenstein, Phys. Rev. D **17**, 2369 (1978); *ibid.* **20**, 2634 (1979).
- [30] H. Nunokawa, J. T. Peltoniemi, A. Rossi, and J. W. F. Valle, Phys. Rev. D **56**, 1704 (1997).
- [31] W. Haxton, Phys. Rev. Lett. **57**, 1271 (1986); S.J. Parke, *ibid.*, 1275 (1986).
- [32] H.A. Bethe, Phys. Rev. Lett. **56**, 1305 (1986).
- [33] G. Sigl and G. Raffelt, Nucl. Phys. B **406**, 423 (1993).
- [34] R. W. Mayle and J. R. Wilson, unpublished (1993).
- [35] G. C. McLaughlin, G. M. Fuller, and J. R. Wilson, Astrophys. J. **472**, 440 (1996).
- [36] G. M. Fuller, R. Mayle, J. R. Wilson, and D. N. Schramm, Astrophys. J., **322**, 795 (1987).
- [37] G. M. Fuller, R. Mayle, B. S. Meyer, and J. R. Wilson, Astrophys. J., **389**, 517 (1992).
- [38] R.F. Sawyer, Phys. Rev. D **42**, 3908 (1990); F.N. Loreti, Y.Z. Qian, G.M. Fuller, and A.B. Balantekin, Phys. Rev. D **52**, 6664 (1995).
- [39] R. Hoffman, S. E. Woosley, G. M. Fuller, and B. S. Meyer, Astrophys. J., **460**, 478 (1996).
- [40] G. M. Fuller, AIP Conference Proceedings **412**, 160 (1997).
- [41] Meyer, B. S., T. D. Krishnan, and D.D. Clayton, **498**, 808 (1998).
- [42] W.C. Haxton, K. Langanke, Y.Z. Qian, and P. Vogel, Phys. Rev. Lett. **78**, 2694 (1997).
- [43] A. B. Balantekin, J. Fetter, G. M. Fuller, and G. C. McLaughlin, Phys. Rev. Lett., to be submitted (1998).

FIG. 1. The geometry in the calculation of the effective neutrino fraction.

FIG. 2. Density is plotted against distance as measured from the center of the neutron star.

FIG. 3. The upper pair of curves shows the actual and equilibrium electron fraction in the absence of any flavor transformation. The lower pair of curves shows the same with neutrino mixing parameters as in Figures 4 and 6. In each pair, the lower line corresponds to the equilibrium Y_e . Above 11 km we include the effects of feedback. Above $Y_e = 1/3$, electron neutrinos may undergo flavor transformation, while below $Y_e = 1/3$ electron antineutrinos may transform. The neutrino driven wind parameters are the same as in Figures 6 and 4. For this dynamical timescale, the actual Y_e closely tracks the equilibrium Y_e . The near complete transformation of electron neutrinos drives the electron fraction to very low values in the lower set of curves. In addition, it almost completely suppresses the alpha effect.

FIG. 4. Electron neutrino (lower curve) and electron antineutrino (upper curve) capture rates on neutrons and protons respectively, plotted against r , the distance from the center of the protoneutron star, for the same choice of parameters as in Figure 6. The $1/r^2$ dependence of the neutrino flux has been removed for illustrative purposes only. All variation seen in the capture rates is due to transformation into sterile neutrinos.

FIG. 5. The potential, V , is plotted against distance (solid line). For comparison we also show V when feedback effects are not included (dotted line). The nearly vertical line at the left edge of the plot corresponds to the inmost $\bar{\nu}_e$ and ν_e resonance at the surface of the neutron star.

FIG. 6. Energy of ν_e s (solid line) and $\bar{\nu}_e$ s (dashed line) undergoing resonance plotted against distance from the center of the protoneutron star, for $\sin^2 2\theta_v = 0.01$, and $\delta m^2 = 20 \text{ eV}^2$, and a dynamical time of $\tau = 0.3 \text{ s}$. For this choice of parameters, electron antineutrinos below $\sim 25 \text{ MeV}$ never undergo a resonance beyond the surface of the neutron star. A resonance may cause a near complete or partial flavor transformation, depending on the adiabaticity.

FIG. 7. Contours of electron fraction at the time of heavy ($A > 40$) element formation, for a range of neutrino mixing parameters δm^2 and $\sin^2 2\theta_v$. The neutrino driven wind timescale is 0.3 seconds. The conditions necessary for a neutron-to-seed ratio of at least 100 are within the $Y_e = 0.18$ (dashed) contour. If no flavor transformation takes place, $Y_e = 0.49$. In the gray region nonradial neutrino paths (not included in this example) may be significant.

FIG. 8. As in Figure 7, but for a timescale of 0.1 seconds. The conditions necessary for a neutron to seed ratio of at least 100 are within the $Y_e = 0.19$ (dashed) contour. If no flavor transformation takes place, $Y_e = 0.47$.

FIG. 9. As in Figure 7, but for a timescale of 0.9 seconds. The conditions necessary for a neutron-to-seed ratio of 100 are within the $Y_e = 0.15$ (dashed) contour. If no flavor transformation takes place, $Y_e = 0.50$.

FIG. 10. The percentage difference in the ν_e capture rate at 11 km, between calculations including and not including the effects of nonradial neutrino paths.

FIG. 11. The potentials, $V(r) \propto \rho(Y_e - 1/3)$, for the two density profiles which we consider. The solid line shows the potential we used for most of our calculations; the dashed line shows the potential for the alternate density profile (see Section IV.B).

FIG. 12. Contour plot generated with alternate density profile. In the grey region nonradial ν paths may be significant. Nonradial paths will not be important at high δm^2 because the potential $V(r)$ turns over at a fairly small value.

Figure 1

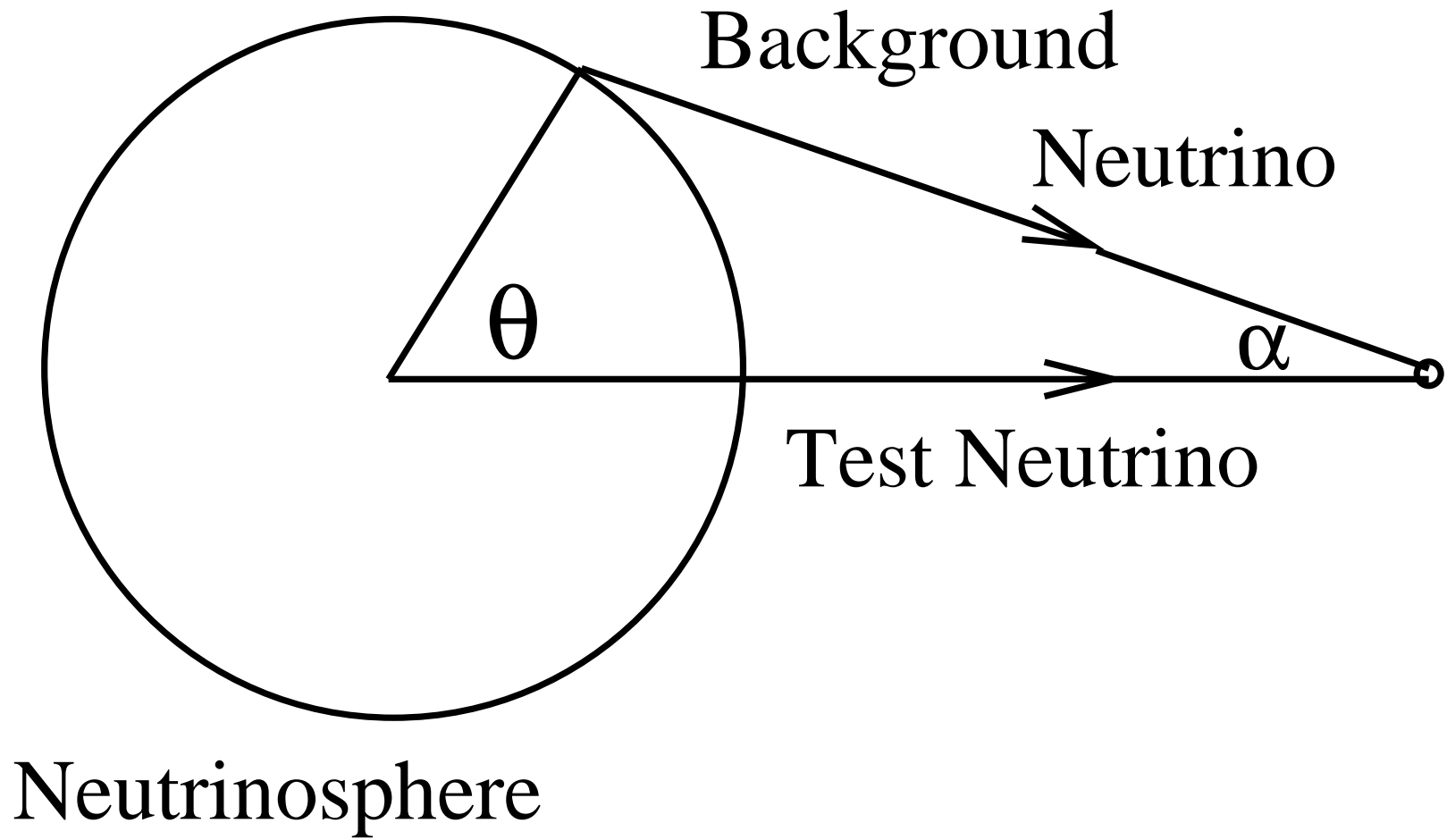


Figure 2

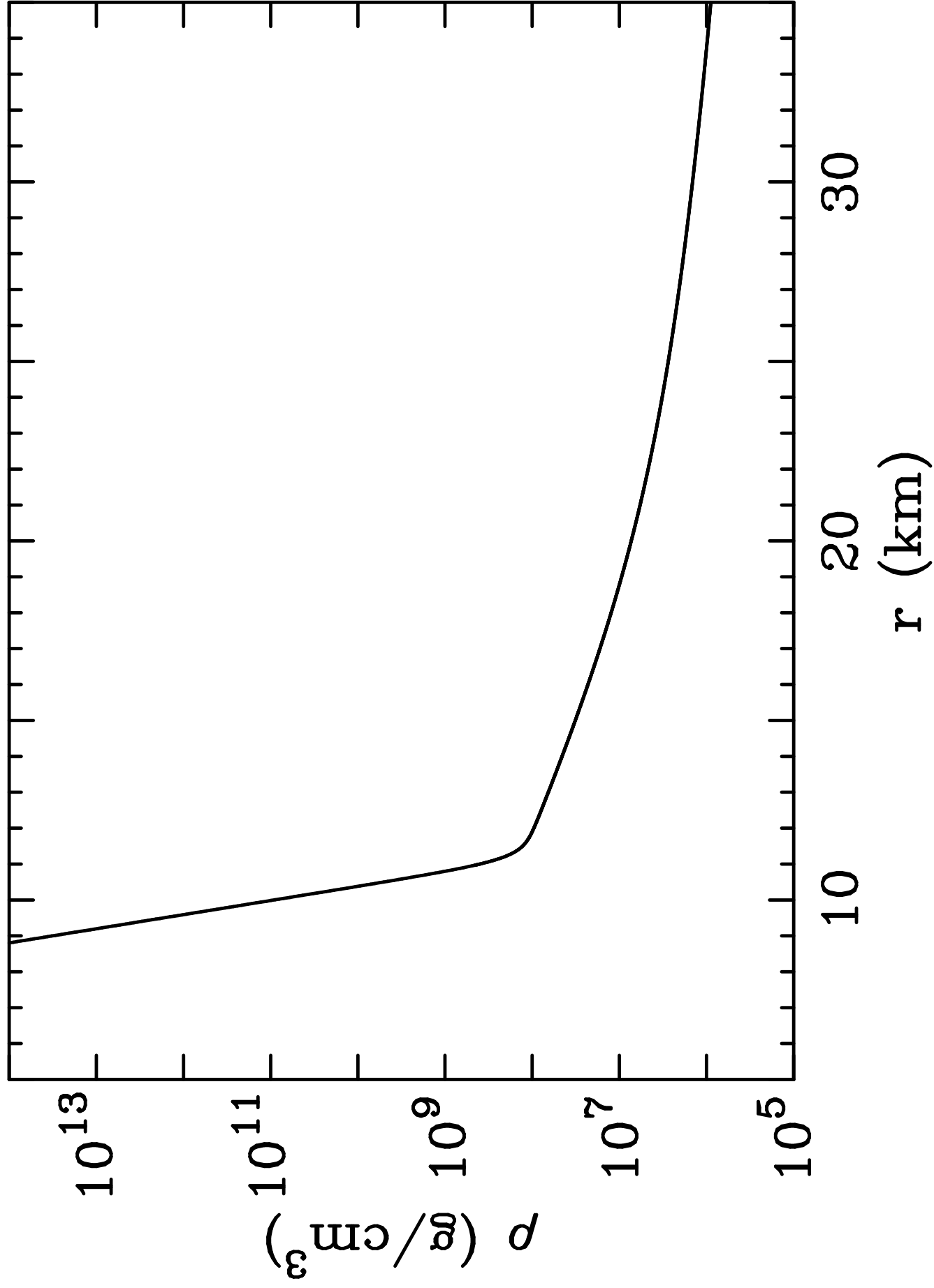


Figure 3

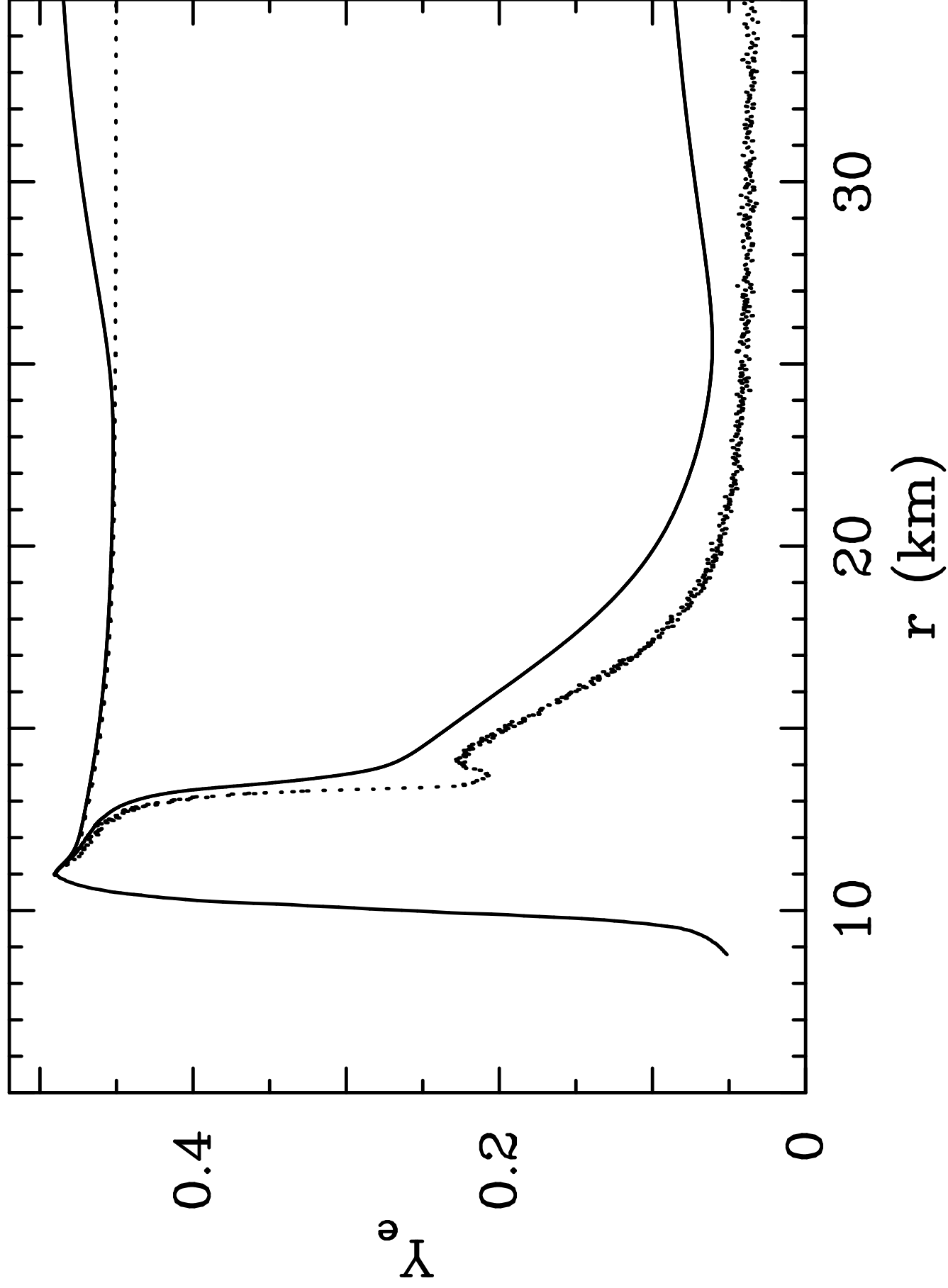


Figure 4

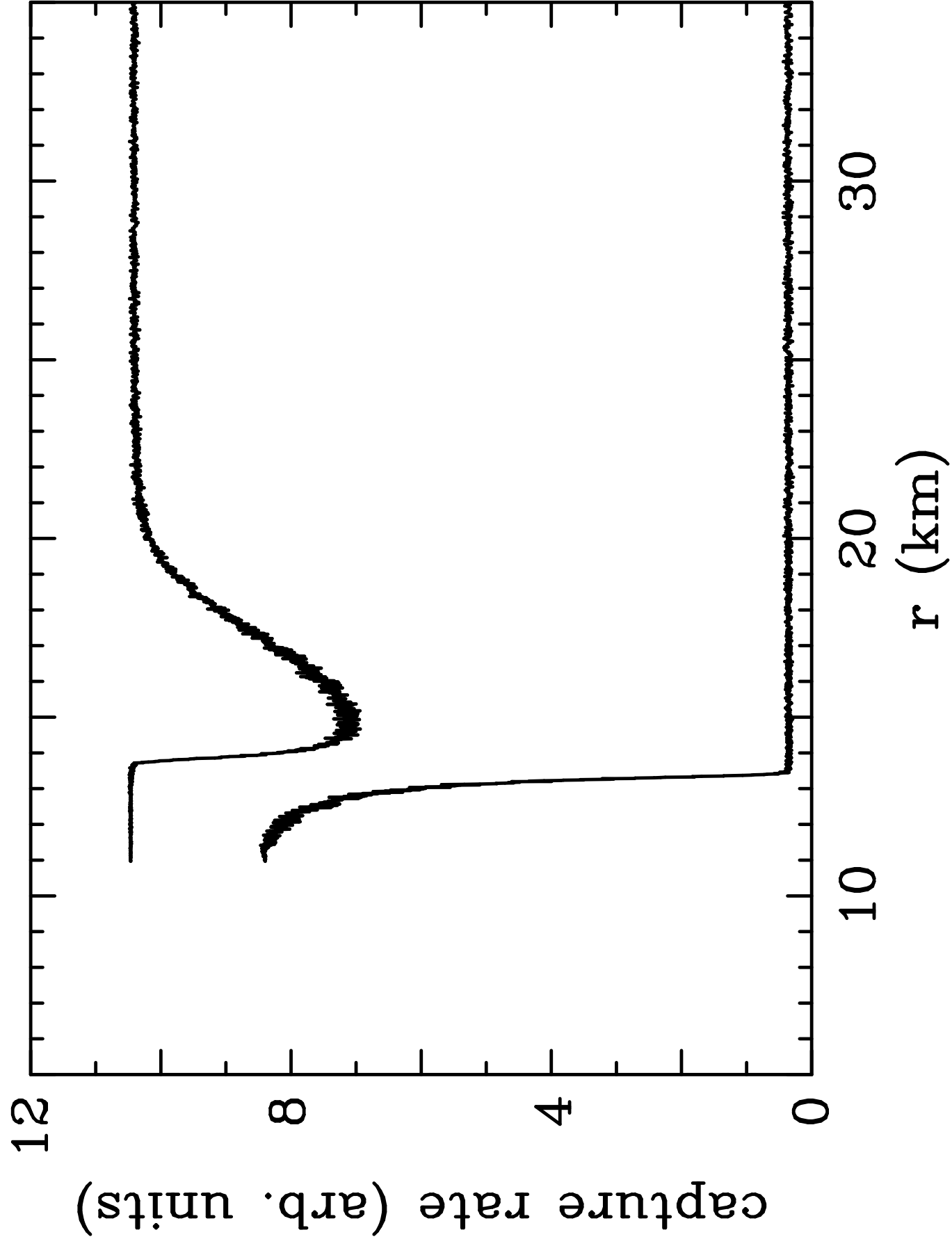


Figure 5

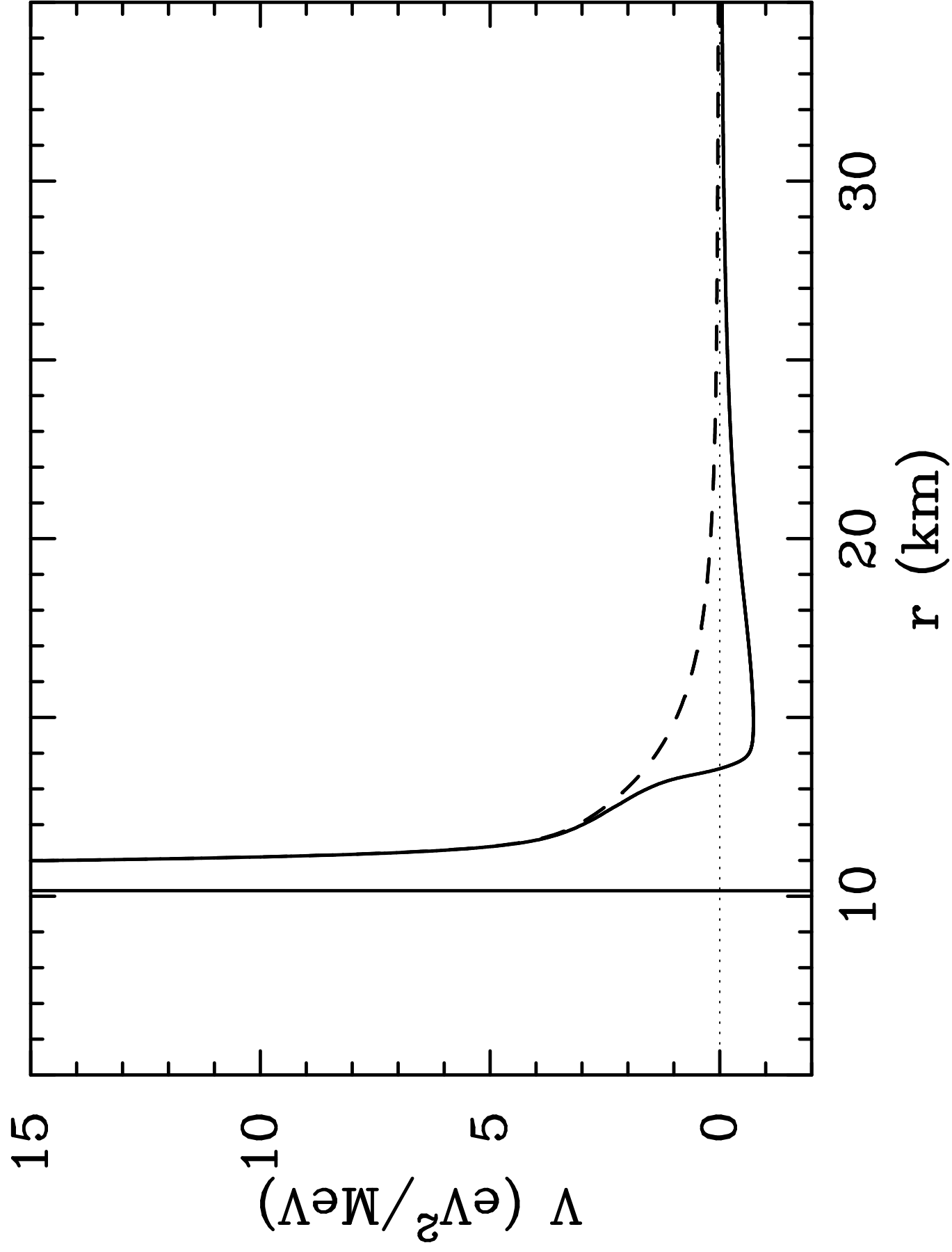


Figure 6

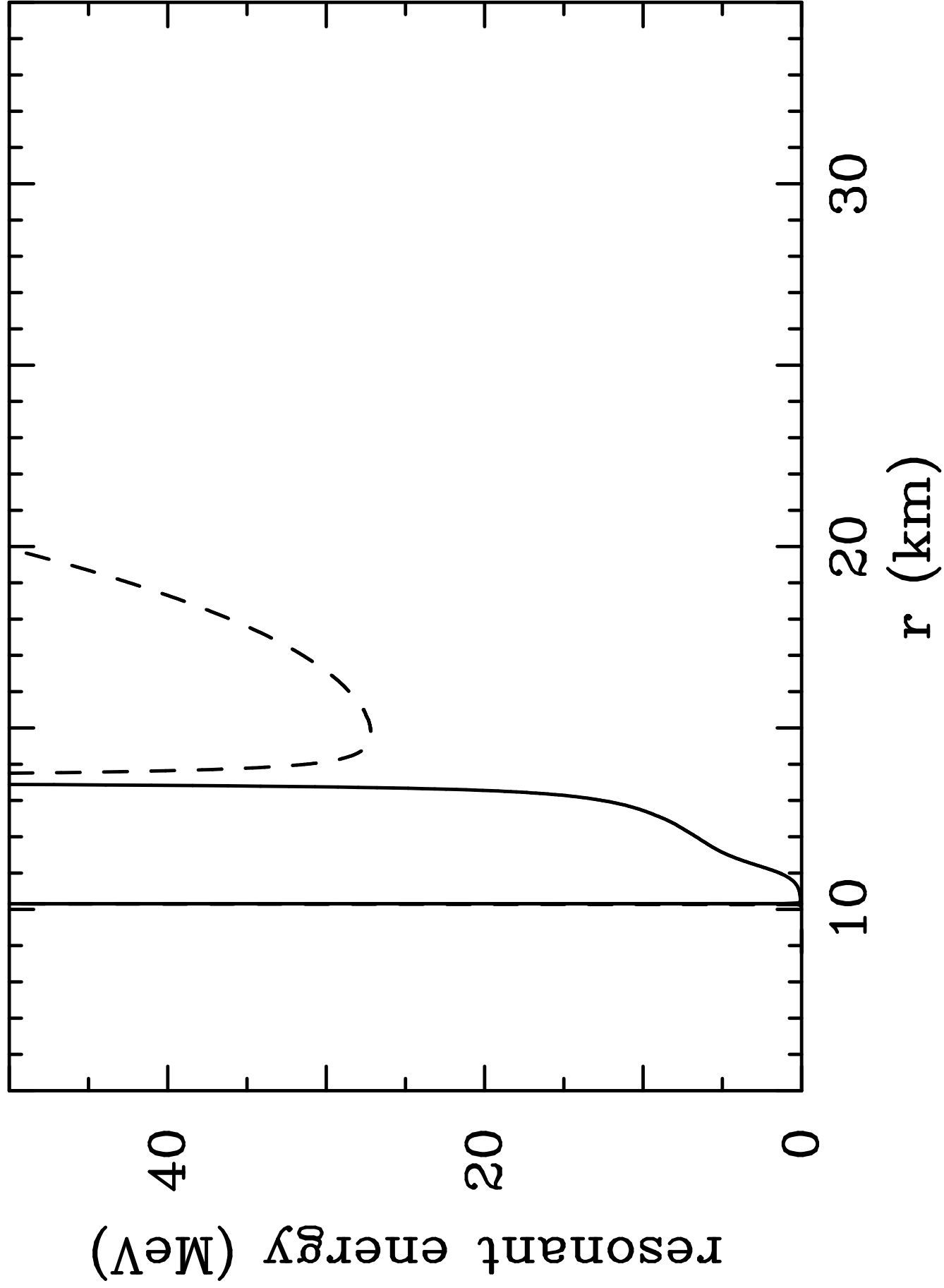


Figure 7

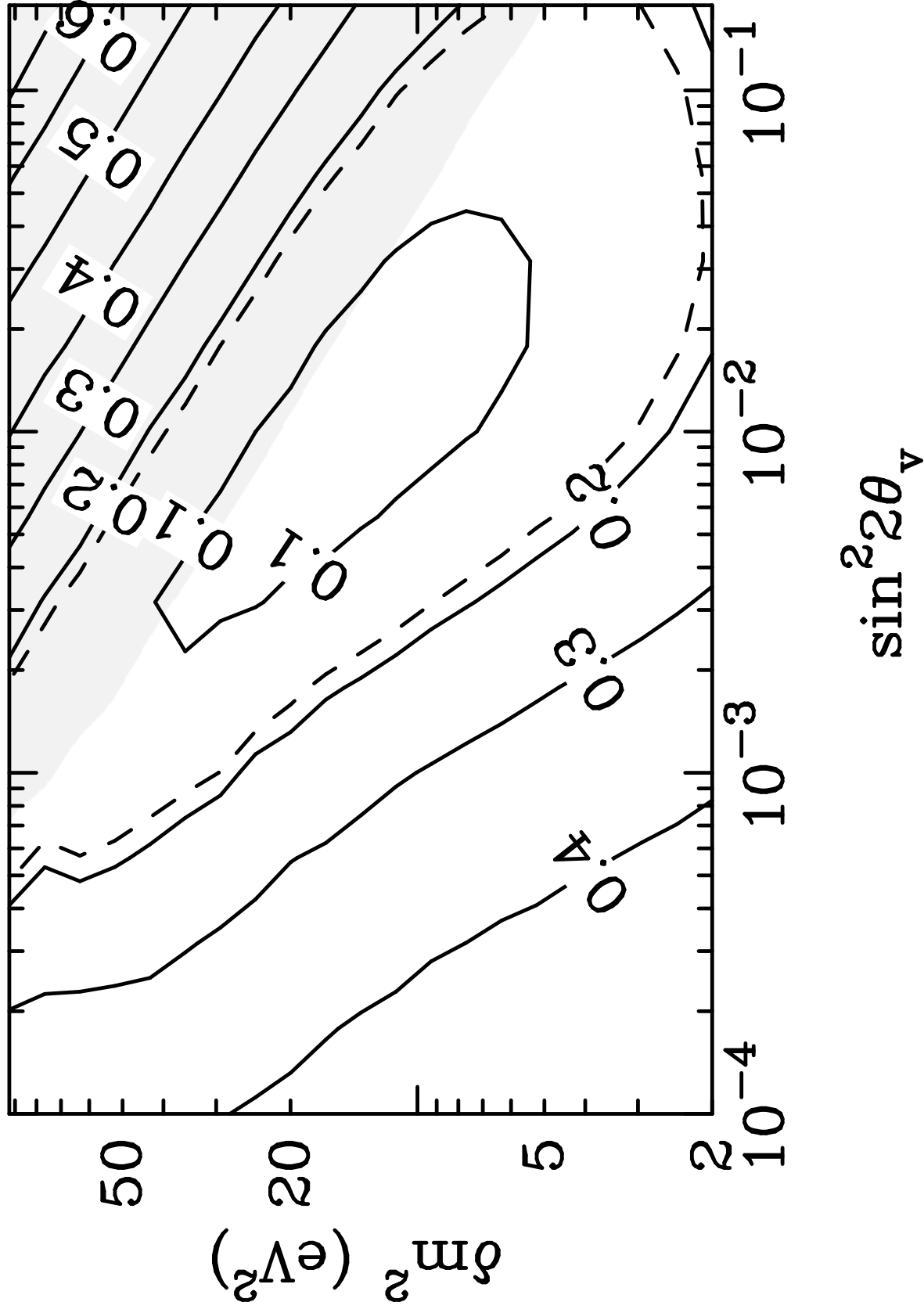


Figure 8

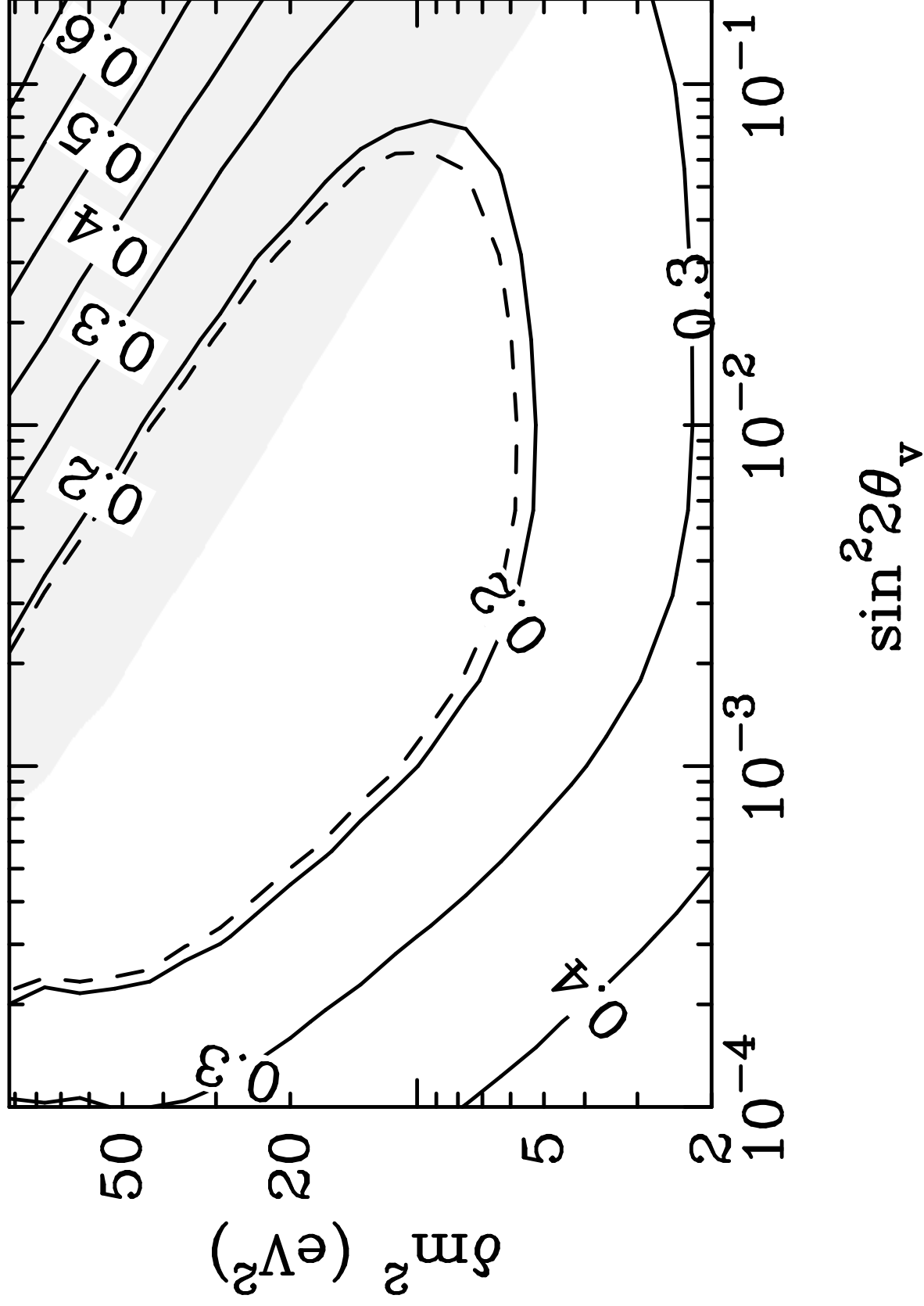


Figure 9

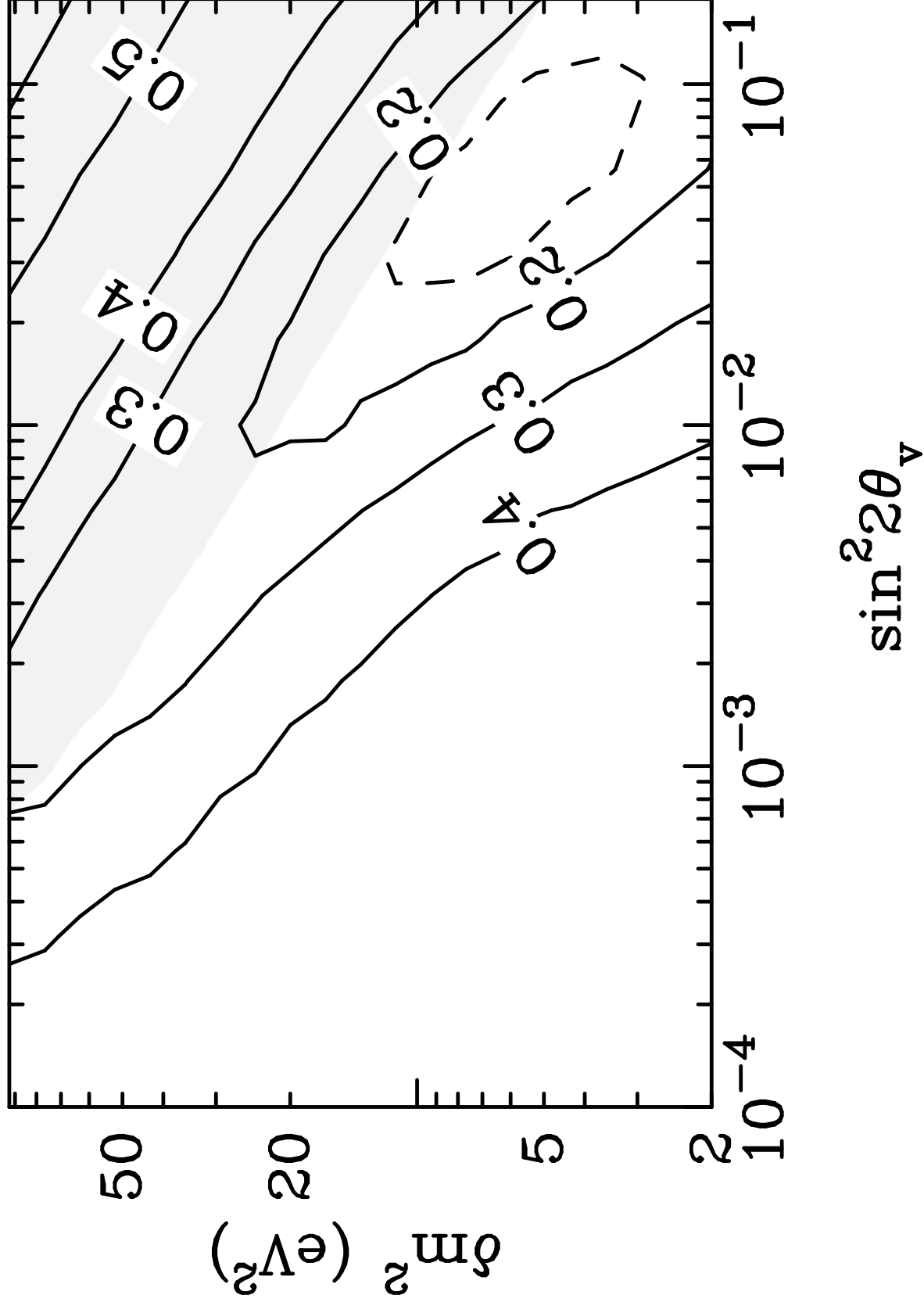


Figure 10

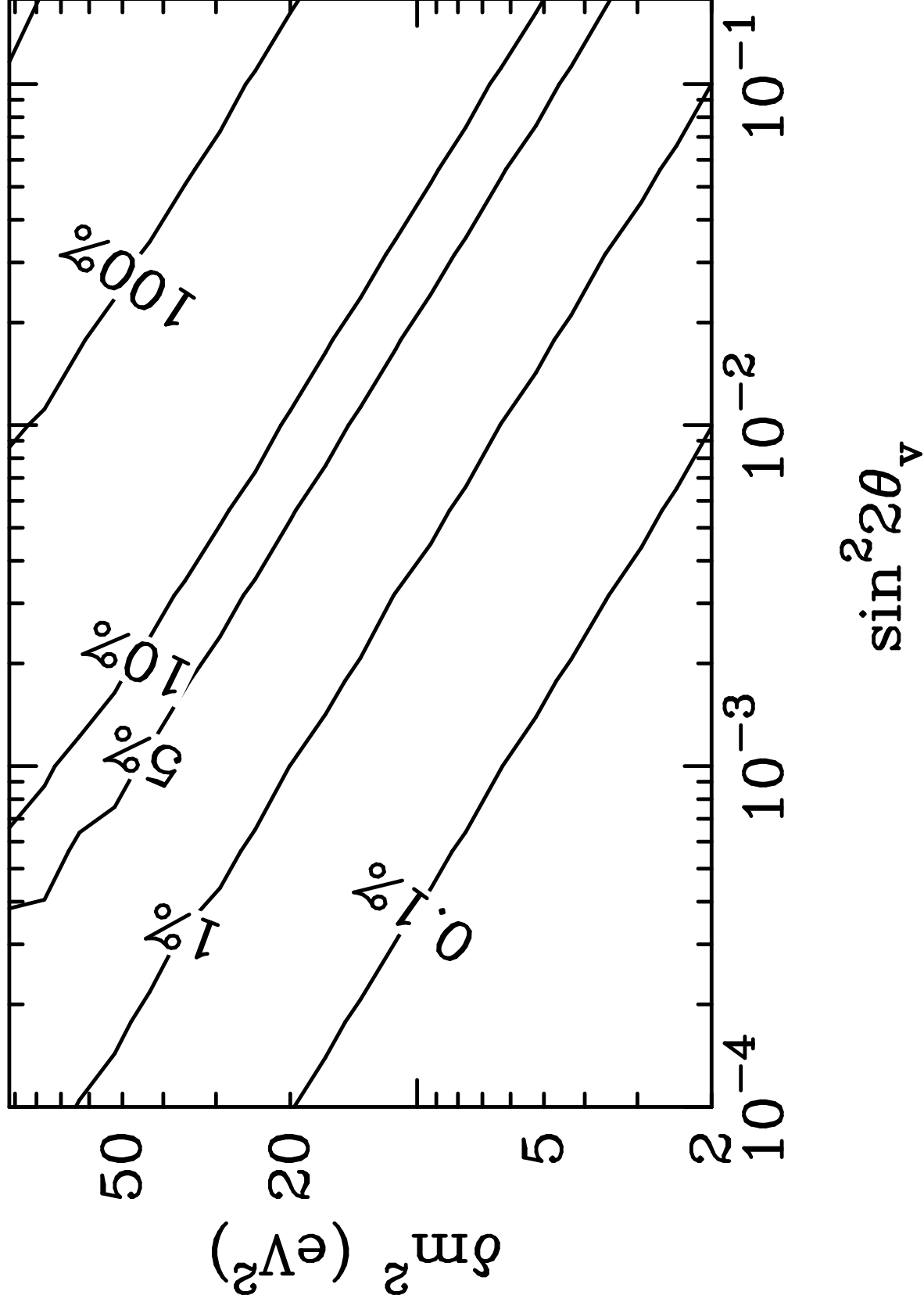


Figure 11

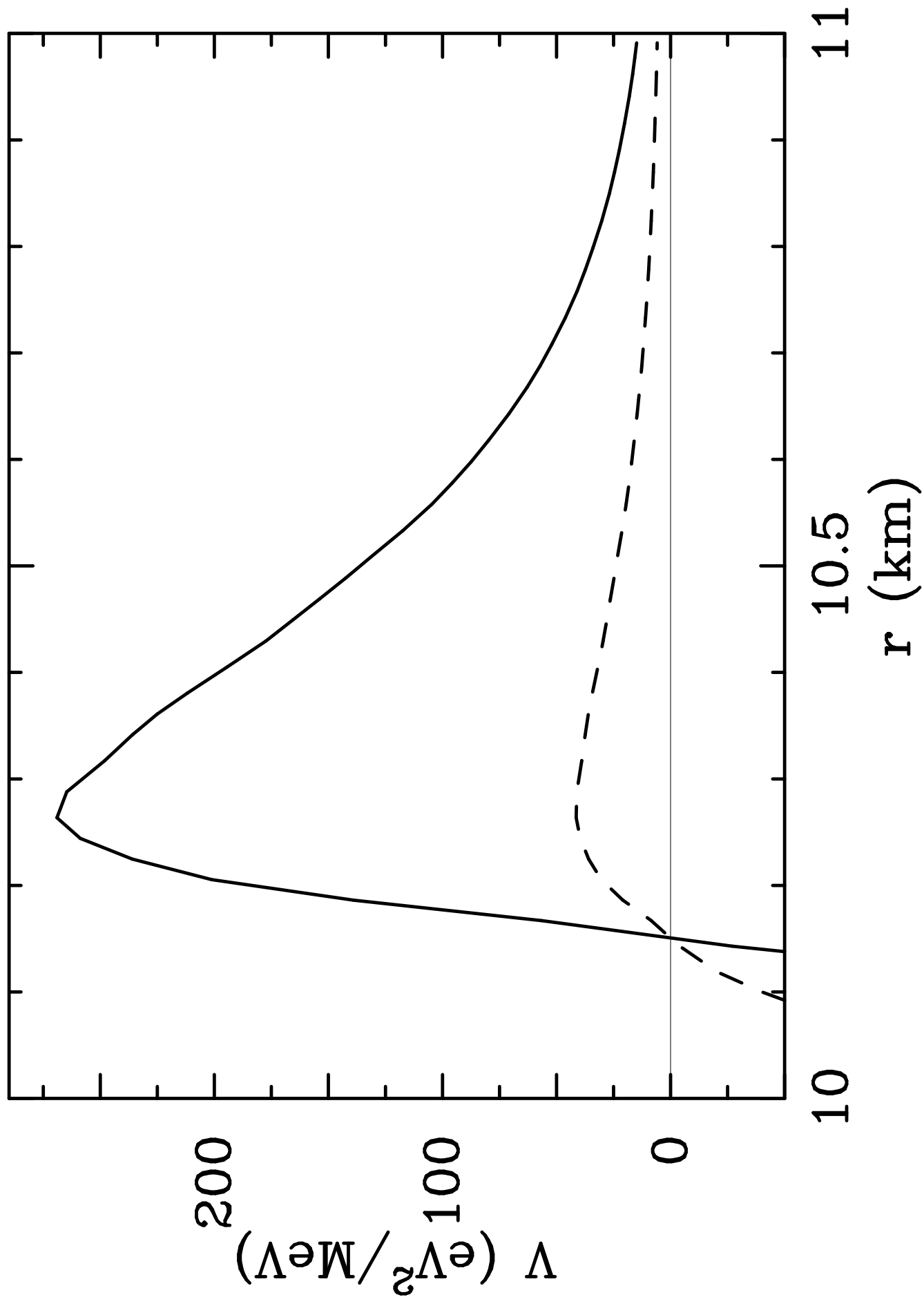


Figure 12

